



---

MSU Graduate Theses

---

Summer 2018

## Application of Nano-Plasmonics for SERS Bio-Detection and Photocatalysis in the Same Platform


Muhammad R. Shattique

*Missouri State University*, sha22@live.missouristate.edu

As with any intellectual project, the content and views expressed in this thesis may be considered objectionable by some readers. However, this student-scholar's work has been judged to have academic value by the student's thesis committee members trained in the discipline. The content and views expressed in this thesis are those of the student-scholar and are not endorsed by Missouri State University, its Graduate College, or its employees.

---

Follow this and additional works at: <https://bearworks.missouristate.edu/theses>

 Part of the [Biology and Biomimetic Materials Commons](#), [Other Materials Science and Engineering Commons](#), and the [Semiconductor and Optical Materials Commons](#)

### Recommended Citation

Shattique, Muhammad R., "Application of Nano-Plasmonics for SERS Bio-Detection and Photocatalysis in the Same Platform" (2018). *MSU Graduate Theses*. 3285.  
<https://bearworks.missouristate.edu/theses/3285>

This article or document was made available through BearWorks, the institutional repository of Missouri State University. The work contained in it may be protected by copyright and require permission of the copyright holder for reuse or redistribution.

For more information, please contact [bearworks@missouristate.edu](mailto:bearworks@missouristate.edu).

**APPLICATION OF NANO-PLASMONICS FOR SERS BIO-  
DETECTION AND PHOTOCATALYSIS IN THE SAME PLATFORM**

A Masters Thesis

Presented to

The Graduate College of  
Missouri State University

In Partial Fulfillment

Of the Requirements for the Degree  
Master of Science, Materials Science

By

Muhammad Rubaiet Shattique

August 2018

Copyright 2018 by Muhammad Rubaiet Shattique

# APPLICATION OF NANO-PLASMONICS FOR SERS BIO-DETECTION AND PHOTOCATALYSIS IN THE SAME PLATFORM

Physics, Astronomy and Materials Science

Missouri State University, August 2018

Master of Science

Muhammad Rubaiet Shattique

## ABSTRACT

Nano-biological systems interfacing nano-structured solid surfaces with biological compounds such as oligonucleotides or proteins are highly regarded as enabling materials for biosensing and biocatalysis applications. In particular, nanostructures of noble metals such as gold or silver, when exposed to light, exhibit a phenomenon known as surface plasmon resonance. When a proper metal nanostructure (plasmonic substrate) is exposed to light, very efficient absorption of incoming photons is possible, resulting in a buildup of localized high-energy regions, or “hot-spots”, where energetic carriers or “hot carriers” can be created. These hot-carriers can be used to catalyze desired chemical transformations in materials located nearby. Furthermore, plasmonic hot-spots are also known to enhance inelastic scattering of light by the same materials, promising multi-functional applications that combine photo-catalytic stimulation of materials with their ultrasensitive characterization in the same design. In this thesis work, we developed a conjugate nano-biological system interfacing plasmonic gold nanostructures with thiolated single-stranded DNA carrying an important reduction-oxidation indicator, methylthioninium chloride, also known as methylene blue. Using surface-enhanced Raman spectroscopy, we have detected characteristic bands of DNA-bound immobilized methylene blue in sub-monolayer quantities. We also have detected reversible reduction-oxidation of methylene blue during laser excitation of the samples at neutral pH, in the absence of electrodes or chemical agents.

**KEYWORDS:** nanoplasmonics, photocatalysis, SERS, nano-bioconjugates, hot-spots

This abstract is approved as to form and content

---

Maria Stepanova, PhD  
Chairperson, Advisory Committee  
Missouri State University

**APPLICATION OF NANO-PLASMONICS FOR SERS BIO-  
DETECTION AND PHOTOCATALYSIS IN THE SAME PLATFORM**

By

Muhammad Rubaiet Shattique

A Master's Thesis  
Submitted to the Graduate College  
Of Missouri State University  
In Partial Fulfillment of the Requirements  
For the Degree of Master of Science, Materials Science

August, 2018

Approved:

---

Maria Stepanova, PhD

---

Kartik C. Ghosh, PhD

---

Keiichi Yoshimatsu, PhD

---

Julie Masterson, PhD: Dean, Graduate College

In the interest of academic freedom and the principle of free speech, approval of this thesis indicates the format is acceptable and meets the academic criteria for the discipline as determined by the faculty that constitute the thesis committee. The content and views expressed in this thesis are those of the student-scholar and are not endorsed by Missouri State University, its Graduate College, or its employees.

## ACKNOWLEDGEMENTS

Throughout the journey of this masters at Missouri State University, I came across many people who have positively impacted my life. I am immensely grateful to them. I am conveying my sincere thanks to Dr. Robert Mayanovic, for letting me use the Raman spectrometer in his research lab. Also to Dr. Kartik Ghosh, Delower Hossain, fellow graduate students and all the friends in Springfield, MO for their love and support.

Special thanks goes to, **Missouri State University**, for giving me the opportunity to study and do research in this wonderful campus. I must mention a few names especially-

**Dr. Maria Stepanova,**

for being my research supervisor and being my mentor. I am very grateful to her. She is an amazing scientist and a teacher. I have learned so much from her.

**Dr. David Cornelison,**

for helping me to succeed through his guidance, support and genuine caring. An amazing human being- I will always look forward to.

**Eiad Hamwi,**

my friend, who has been there in my ups and downs, always. A gem of a friend.

**Devon West-Spheling,**

to help me change my old ideas about life, career and success.

**Rishi Patel,**

for letting me use the facilities at the JVIC and always helping with my research questions. He helped me with my substrate preparation and characterization immensely.

**My parents,**

who have sacrificed a lot for me. This one is for them.

## TABLE OF CONTENTS

Chapter One: Introduction .....	1
Chapter Two: Literature Review .....	3
2.1 Nanoplasmonics .....	3
2.2 Raman Scattering of Light .....	5
2.3 Surface Enhanced Raman Spectroscopy.....	8
2.4 Applications of SERS.....	9
2.5 Multifunctional Applications of Nano-plasmonics.....	11
Chapter Three: Objectives.....	16
Chapter Four: Methods .....	17
4.1 Instruments Used for Plasmonic Substrate Fabrication and Characterization.....	17
4.2 Instruments and Chemicals used for Biofunctionalization.....	26
Chapter Five: Results .....	28
5.1 Protocols Used To Fabricate Nano-Bio Conjugate System.....	28
5.2 Benchmark Raman and SERS Characterization of All Components Experiment.....	33
5.3 SERS detection of reduction-oxidation processes stimulated by LSPR hot- spots under laser excitation.....	37
Chapter Six: Discussion.....	43
Chapter Seven: Conclusions.....	46
References.....	48

## LIST OF FIGURES

Fig. 2.1. Schematic Energy diagram explaining the Raman Effect.....	6
Fig. 2.2. Schematic diagram of a Raman experiment setup .....	7
Fig. 2.3. Typical Raman Spectrum of water on a silicon substrate.....	8
Fig. 2.4. A schematic diagram of SERS arrangement. ....	9
Fig. 2.5. (a) Schematic and (b) energy diagram showing the generation process of plasmonic hot carriers by light-induced excitation of SPR on a metal nanoparticle.....	12
Fig. 2.6. Thermal driven and electron driven reactions. (a) Di-atomic molecules are dissociated through thermal activation. (b) The dissociation of di-atomic molecules with the help of electrons. (c) When the incident flux of photon is high, electron can get injected in the di-atomic molecule before the molecular vibration is dissipated completely. (d) Plasmonic metal nanoparticles induce electron-driven reactions (top), which can trigger certain chemical reaction pathways that are not accessible otherwise (bottom). ....	14
Fig. 2.7. Plasmonic light-trapping geometries for thin-film solar cells. (a) Light is trapped through scattering from metal nanoparticles at the surface of the solar cell. (b) Light can be trapped when it excites localized surface plasmons in metal nanoparticles embedded within the semiconductor. (c) When the excitation of surface plasmon polaritons occurs at the metal/semiconductor interface, light also is trapped.....	15
Fig. 4.1. Emitech K550X sputter coater from Quoram Technologies (Adapted with permission from Quoram Technologies).....	18
Fig. 4.2. Sonication bath.....	20
Fig. 4.3. Plasma Etcher.....	21
Fig. 4.4. Horiba LabRAM HR 800 Evolution Raman spectrometer.....	22
Fig. 4.5. Raman spectroscopy setup: A 10x microscope is exposing 532 nm laser on a substrate.....	23
Fig. 4.6. Schematic of the experimental setup of Raman spectroscopy of liquid Samples.....	24
Fig. 4.7. Taurus mpc300 532nm Green lase by Laser Quantum.....	26



Fig. 4.8. Oxidized (top) and reduced (bottom) structures of methylene blue.....	27
Fig. 5.1. Au coated glass substrate preparation steps.....	29
Fig. 5.2. AFM surface morphology of Au coated glass substrates at different coating thickness (5nm -30nm).....	30
Fig. 5.3. AFM 3-D topographical image of Au coated glass substrates at different coating thickness.....	31
Fig. 5.4. Scheme of DNA functionalized, gold-coated plasmonic substrate.....	32
Fig. 5.5. Steps of substrate bio-functionalization with DNA and methylene blue.....	33
Fig. 5.6. Benchmark Raman spectrum of Tris-EDTA buffer on Au coated glass substrate. No characteristic peaks observed.....	34
Fig. 5.7. Raman spectrum of ss-DNA incubated on gold coated glass slide.....	35
Fig. 5.8. Raman spectrum of methylene blue solution on gold coated glass substrate without incubation.....	36
Fig. 5.9. Raman spectrum of rinsed gold-coated glass substrate after a 24 h incubation with methylene blue in the absence of DNA functionalization.....	37
Fig. 5.10. SERS spectrum of DNA-functionalized, MB-loaded gold coated glass substrate after a 24 h incubation and rinsing.....	38
Fig. 5.11. SERS spectra of DNA-functionalized, MB-loaded gold-coated glass substrate at the beginning of a 523 nm laser exposure (bottom); after 100 min of the exposure (middle); and after 140 min of the exposure following the addition of Tris-EDTA buffer (top). A vertical offset was applied to the spectra for clearer presentation.....	40
Fig. 5.12. Reduction-oxidation cycle of Methylene blue at neutral pH and in absence of electrode potential on Au coated glass plasmonic substrates.....	41
Fig. 5.13. Raman spectra of a drop of MB solution on a bare uncoated glass slide at the beginning of laser exposure (bottom); after 100 min of the exposure (middle); and after 140 min of the exposure following the addition of Tris-EDTA buffer (top). A vertical offset was applied to the spectra for clearer presentation.....	42

Fig. 5.14. Raman spectra demonstrating electrochemically-driven reduction-oxidation of MB. Reduction of MB : (a) With increasing negative electrode potential, the characteristic peaks of MB dies down and disappears at  $\sim -500$  m V. Oxidation of MB: (b) When the potential is reversed the characteristic peaks starts reappearing.....45

## CHAPTER ONE: INTRODUCTION

Light is our abundant source of energy. With growing population, increasing dearth of bio-mass based fuels and increasing environmental pollution due to greenhouse gases, light harvesting in order to store energy and using it subsequently has become a pressing demand of our time. Plasmonic nanostructures are very promising materials to harvest the energy of light. In particular, nanostructures of noble metals such as gold or silver, when exposed to light, exhibit a phenomenon known as surface plasmon resonance. Surface plasmons are oscillations of electron density at a surface of a metal. When a proper metal nanostructure (plasmonic substrate) is exposed to light, very efficient absorption of incoming photons is possible, resulting in a buildup of localized high-energy regions, or “hot-spots”, where energetic carriers or “hot carriers” can be created. Energy of hot-spots may be used in a variety of ways, such as for example- inducing reduction-oxidation responses in biological materials. Furthermore, plasmonic hot-spots are also known to enhance inelastic Raman scattering of light by materials located nearby. The surface-enhanced Raman spectroscopy (SERS) allows capturing unique vibrational fingerprints of materials in sub-monolayer quantities, and as such it is highly regarded as a method of ultra-sensitive and selective bio detection. Combining energy harvesting from light, photo-catalytic stimulation of materials, and ultrasensitive SERS characterization of molecular events in the same design promises numerous transformative applications.

This research work is an experimental work, which demonstrates a multifunctional application of plasmonic nanostructures. In this research, we have devised a way of synthesizing plasmonic nano-structures in a simple way. Also, we have devised a way of bio functionalizing of these plasmonic substrates that is suitable for immobilizing molecules from solutions. We were able to immobilize a pigment known as Methylene Blue (MB) from a solution on our substrates. Then, we detected sub monolayer quantities of the pigment by Surface Enhanced Raman Spectroscopy (SERS) technique. Furthermore, we carried out chemical modification (reduction-oxidation) of the immobilized pigment on our plasmonic substrates by merely exposing them to laser light at neutral pH and without the application of electrode potential. We successfully monitored these chemical changes on the same system using SERS.

## CHAPTER TWO: LITERATURE REVIEW

### 2.1 Nanoplasmonics

Metals are bonded through metallic bonding, which is a result of the electrostatic attractive forces between electrons and metal ions that eventually form bulk metals. In a metal, valence electrons are detached from metal ions, which form a periodic lattice. The valence electrons are shared over the entire metal volume, such that the metal ions are immersed in a “sea” of mobile valence electrons. The strength of metallic bonding is related to the density of these delocalized electrons (Anker et al., 2008a). However, when the size of metals is less than the wavelength of light their properties also change. Usually, the electrons have a mean free path of 40nm-50nm in noble metals such as Gold (Au) (Bantz et al., 2011b). Nanoparticles of these noble metals can be synthesized with sizes less than 50 nm (Sylvia, Janni, Klein, & Spencer, 2000). When an electromagnetic (EM) wave such as light is incident on nanoparticles, it interacts with their surface. If the frequency of the incident photons is close to the plasma frequency of the free electrons on the surface of metal nanostructures, it will lead to a collective oscillation commonly known as the localized surface plasmon resonance (LSPR). (Barnes, Dereux, & Ebbesen, 2003; Homola, Yee, & Gauglitz, 1999). Surface plasmons are resonant oscillations of conduction electrons in nanoparticles exposed to light. The collective oscillation of electrons results to an enhancement of the local EM field, which is predominantly confined to the metal surface. Following the resonant excitation, the Plasmon decays within tens of femtoseconds. The decay can take place through radiative photon emission

(i.e., scattering) and/or through generation of energetic charge-carriers at the nanoparticle surface. These energetic electron-hole pairs are termed hot electrons/holes (Ye, Long, Huang, & Xiong, 2017). The shape and size of nanoparticles determine the electron density, which in turn determines plasmonic oscillations (Cheng, Mayes, & Ross, 2004). For example, the dielectric constant of environment can influence plasmonic oscillations of electrons (Cheng et al., 2004).

When two closely positioned metal nano-particles are exposed to light, a localized electromagnetic field is formed between and around the nanoparticles. This localized EM field is termed as 'Hot spots' in the field of nano-plasmonics (Cheng et al., 2004). Thus synthesis of nanostructures that can maximize the hotspot generation has been addressed extensively in the recent years (Xie & Schlücker, 2014). The plasmonic substrates can be fabricated through vapor synthesis techniques such as thermal evaporation, or magnetron sputtering of noble metals on glass substrates. The roughness of the deposited metal and the close proximity between neighbor crystallites are often sufficient to generate hotspots. Due to randomness of such structure, control over size and location of hotspots is limited. Compared to such easy to use but difficult to control techniques, nanolithography presents the opportunity of a greater control over nanostructures (Dieringer et al., 2006). Nano-sphere lithography (Giljohann et al., 2010; Li et al., 2018) and electron beam lithography (Peters, Gutierrez-Rivera, Dew, & Stepanova, 2015) are the most common lithographical techniques used to produce plasmonic nanostructures. Other methods used to create controlled nanostructures include block co polymer template synthesis (Peters et al., 2015) and selective etching of bimetallic nanoparticles (Peters et al., 2015). Another promising way to produce plasmonic substrates is by self-

assembly of colloidal nanoparticles. The key in success of this method is to functionalize nanoparticles in a way that can tune their aggregation propensity (Peters et al., 2015). For example, DNA functionalization of nanoparticles to create tunable nanostructures that can generate plasmonic hotspots have been vigorously researched and very successful (Cao, Jin, & Mirkin, 2002b; Mirkin, Letsinger, Mucic, & Storhoff, 1996).

## **2.2 Raman Scattering of Light**

Sir C. V. Raman and K.S. Krishnan together discovered that the light can scatter from materials with a change in frequency (Raman & Krishnan, 1928) (Fig.2.1). The shifts in frequency depend upon the molecules light interacts with. The differences in wave number between the incident radiation and the scattered light are related to vibrational and rotational energy states of the molecules. In contrast, elastic scattering of radiation by matter occurs without frequency shift. Known for a long time as the "Rayleigh" or "Tyndall" scattering, elastic scattering explains, for example, the blue color of the sky. However, the "Raman effect" has been discovered significantly later because of the low probability of its occurrence during interactions between photons and molecules. Only one in  $10^6 - 10^{10}$  photons would undergo inelastic scattering (Raman & Krishnan, 1928).

In Raman Effect the interaction is not a simple act of fluorescence. During fluorescence a molecule absorbs a photon, and another one of different frequency is emitted. In that case, the incoming radiation is actually absorbed by the molecule. In contrast, in the Raman Effect such an absorption is not necessary.

The Raman Effect is utilized in the spectroscopy technique called the Raman spectroscopy, which is a very useful and versatile non-destructive characterization technique. Raman spectra are representative of vibrational characteristics of a material. Since Raman spectroscopy can detect various modes of molecular vibrations, it captures unique vibrational fingerprints of many materials including crystalline solids, non-crystalline solids, biological species, liquids, thin films, etc.

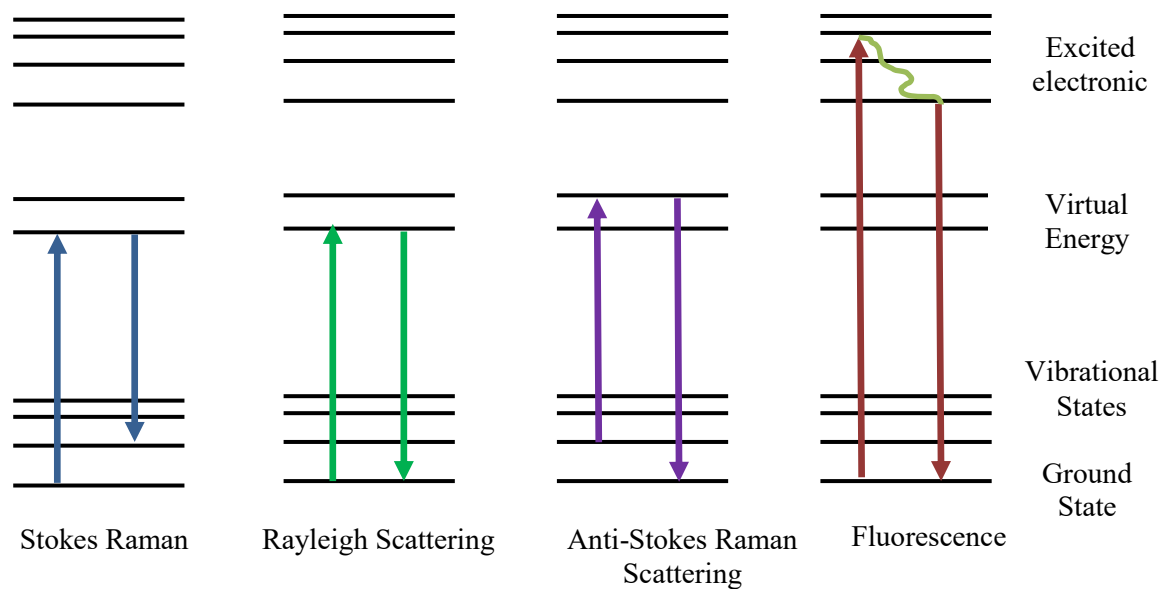


Fig. 2.1. Schematic Energy diagram explaining the Raman effect (Haynes, McFarland, & Duyne, 2005)

A simplified setup of Raman Spectroscopy consists of monochromatic filter (excitation filter) which allows only light with a specific wavelength to reach the sample. The measured scattered light exhibits a broader spectrum of wavelengths. A second filter (emission filter) behind the sample allows blocking of the incident wavelength. This allows to separate observed scattered light from the incident light (Fig. 2.2).



The light source of a Raman spectrometer is in general a laser with a specific wavelength. The laser's wavelength typically ranges from 400 nm to 800 nm depending on the application. In Raman spectra, the intensity of measured Raman scattering is plotted versus the frequency shift. The Raman frequency shift is defined as a difference between the measured frequency of scattered light and incident light. Therefore, Raman spectra are independent of the wavelength of the light source. However, instead of using the wavelength, the Raman shift is conventionally given as change of the wavenumber ( $\text{cm}^{-1}$ ) which is inversely proportional to the wavelength. The intensity of scattered light is plotted against the wavenumber in a typical Raman spectrum. For example, Fig. 2.3. shows a Raman Spectrum of water on a Si substrate. The intensity of scattered light is plotted as a function of a shift in frequency here. Characteristic Raman bands of water ( $3200 \text{ cm}^{-1}$ - $3500 \text{ cm}^{-1}$ ) and silicon ( $530 \text{ cm}^{-1}$ ) are clearly seen in this plot.

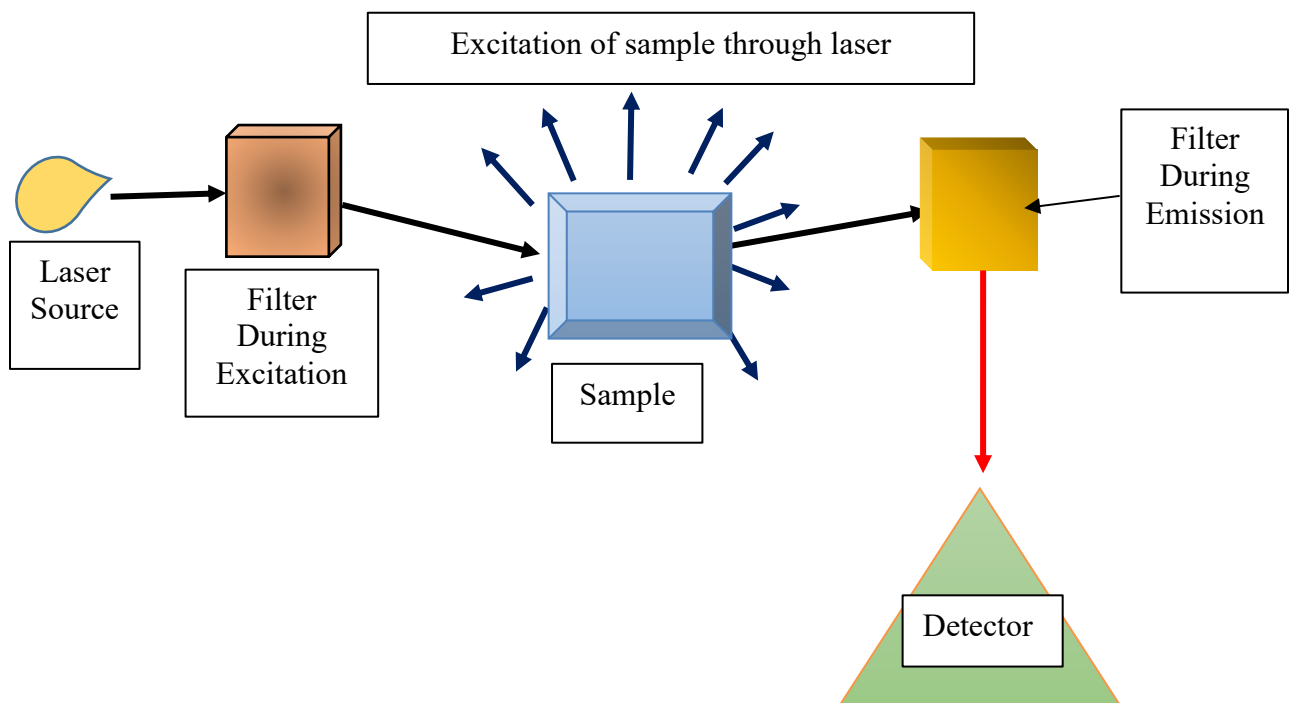


Fig. 2.2. Schematic diagram of a Raman experiment setup (Knight & White, 1989)

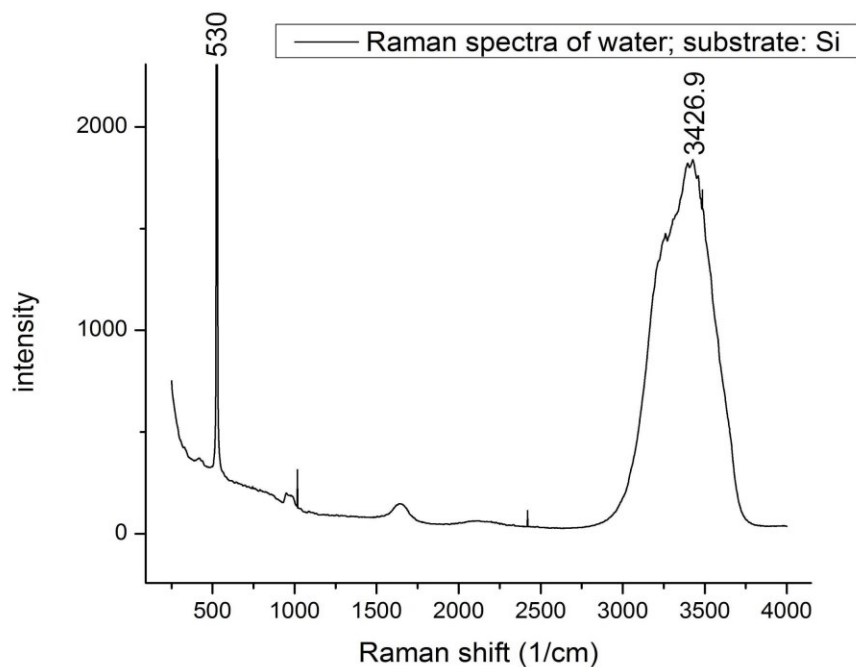


Fig. 2.3. Typical Raman Spectrum of water on a silicon substrate.

### 2.3 Surface Enhanced Raman Spectroscopy (SERS)

The Raman scattering is enhanced by the presence of plasmonic nanostructures (Haynes et al., 2005) (Fig. 2.4.). Hot-spots generated by these nanostructures interact with the Raman scattering, and this interaction results in a  $10^3$ - $10^6$  times enhancement of the inelastic scattering (Sharma, Frontiera, Henry, Ringe, & Van Duyne, 2012; Zeng, Liu, & Wei, 2016). The origin of this enhancement effect is still debatable. Two models have been proposed to explain Surface-Enhanced Raman Scattering (SERS), Chemical enhancement and Electromagnetic field enhancement (Sharma et al., 2012). According to the chemical enhancement model, the nature of the molecules that interact with light

determines the enhancement factor. Different chemical environment around the same molecule will produce a different enhancement effect depending on its chemical composition. The localized EM field in the hot spots plays a key role in the enhancement of the Raman Effect according to the electromagnetic field enhancement model. The size, shape and interparticle distance can influence the localized EM field strength, thus influencing the overall scattering enhancement (Zeng et al., 2016).

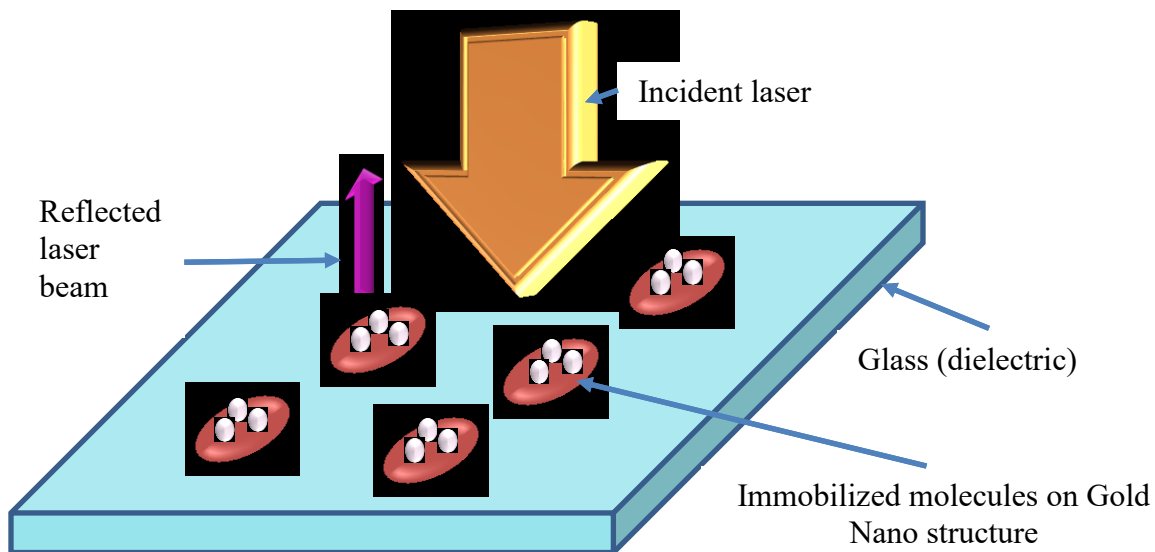


Fig. 2.4. A schematic diagram of SERS arrangement. (Peters et al., 2015)

## 2.4 Applications of SERS

For regular Raman spectroscopies, a large number of molecules are required to generate enough scattered photons to be detected. For example, if one uses a 100mW laser with a 1  $\mu\text{m}$  of laser focus area, a single molecule will emit only  $10^4$  photons per

second. This is a very small amount, which will in turn make the experimentalist to wait more than an hour to detect a single scattered photon. SERS enhances the photon signal significantly amount, which enables the observer to detect Raman photons coming from a single molecule more easily (H. Liu et al., 2011). This effect has been instrumental for fingerprint detection from monolayers of molecules (Ravindran, Chandran, & Khan, 2013). Detection of nano-sized biological entities such as DNA, and even identification of individual bases Adenine, Guanine, Cytosine, or Thymine was accomplished using SERS (Cao, Jin, & Mirkin, 2002a). Moreover, living entities such as living cells can be detected using SERS too (Cao et al., 2002a). This means that plasmonic nanostructures that utilize SERS can be effective biosensors (Bantz et al., 2011a). This paves the way of in vivo spectroscopy of living organisms. Besides, SERS has been utilized to detect chemical warfare agents. With the development of portable Raman spectrometers, this technique can be used for the security purposes (Brosseau, Casadio, & Van Duyne, 2011). SERS can be used in electrochemistry also. Many chemicals change their oxidation states with the change of potentials, and these oxidation states can be detected through SERS because different oxidation states has different vibrational frequencies (Oakley, Dinehart, Svoboda, & Wustholz, 2011). Chemical present in a very small amount is of huge interest in preserving old art pieces and detecting imitations. SERS has been used in this field extensively (Roh, Matecki, Svoboda, & Wustholz, 2016). SERS is also used in ultrafast and femtosecond spectroscopy with the idea that noble metal nanostructures that enhance the Raman signals also allow to detect charge transfer mechanisms in molecules precisely (Paxton, Kleinman, Basuray, Stoddart, & Van Duyne, 2011). In nano-bioconjugates plasmonic nanostructures are functionalized by a biological

entity. So far, these nanobioconjugates sensors have been used for DNA/Aptamer based sensing, protein/enzyme/peptide/antibody SERS biosensing, cellular and in vivo sensing (Weitz, Garoff, Gersten, & Nitzan, 1983). One can extract both qualitative and quantitative information from the SERS spectra.

## **2.5 Multifunctional Applications of Nano-plasmonics**

Free electrons on the metal surface can have strong interactions with incident photons as discussed in section 2.1. Surface plasmon resonance is a powerful tool to concentrate light at the metal–dielectric interface. Thus, plasmonic metal nanostructures offer high capabilities for light trapping and electromagnetic field enhancement. The surface plasmon resonance has potential applications in photo catalysis (Ye et al., 2017) and photovoltaics (Kulkarni, Noone, Munechika, Guyer, & Ginger, 2010) and sensing (Anker et al., 2008b) as well as in surface-enhanced Raman scattering (SERS) as discussed in previous section

In a photo-catalysis process solar energy is converted to chemical energy. This energy is usually stored in chemical bonds of molecules. In a typical photocatalytic process, light of appropriate energy is absorbed. This absorbed energy excites the electrons, which in turn generates photo-excited electrons and holes. The photo-generated electron–hole pairs are then separated and transferred to the surface. These electron–hole pairs take part in reduction-oxidation reactions. The photocatalytic effects of nano plasmonics can be used in water splitting, carbon di-oxide reduction, degradation of organic pollutants etc. (Ye et al., 2017). Plasmon-assisted photo catalysis is very promising as it selectively oxidizes organic substrates. Traditional catalytic oxidation

processes usually occur under high temperature, pressure and/or extreme pH conditions. In the case of nano-plasmonics- the hot carriers that are generated, may influence the oxidation mechanism by favoring the adsorption of intermediate species and/or of oxidizing agents. This significantly improves selectivity of the reaction. (Kim, Lee, Moon, & Park, 2016a)

Hot electrons at the metal surface are generated in several steps (Kim et al., 2016a). First, the metallic nanostructure is excited using light; this light has a much larger wavelengths than the size of metal nanoparticles. Next, the excited charges can decay either radiatively into a photon (scattering) or nonradiatively into hot carriers. Non radiative decay is considered as an effective pathway for generating hot electrons at the metal surface. Eventually, these hot electrons transfer their energy into specific electronic states of molecules that are adsorbed on the metal surface through many different ways (Persson & Ryberg, 1981). This phenomenon may take place prior to losing the energy of hot-electros by either electron–electron scattering or electron– phonon coupling at a femtosecond to picosecond time scale (Fig. 2.5.) (Kim, Lee, Moon, & Park, 2016b) .

Plasmon driven photo-catalysis can occur through thermal pathways or directly by hot-carriers (Kim et al., 2016b). A large number of reactions such as ammonia synthesis, hydrocarbon reforming, oxidation and hydrogenation reactions are thermally activated processes that can be thermally catalyzed using metal NPs. Thermal catalysis on metallic surface is primarily a process which is phonon-driven. Decay of hot electrons can activate phonon modes of the metal.

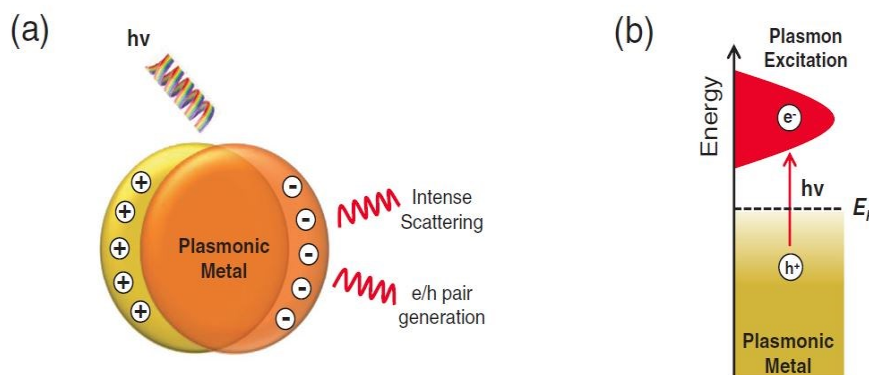


Fig. 2.5. (a) Schematic and (b) energy diagram showing the generation process of plasmonic hot carriers by light-induced excitation of SPR on a metal nanoparticle. Reproduced with permission from Ref (Kim et al., 2016b).

Then absorbed molecules' vibrational modes couple with the phonon modes of the metal. In such case, different thermal activation pathways are possible. This usually results in a large number of unwanted by-products. In contrast, direct plasmonic photocatalysis tends to promote selective chemical reactions, thus overcoming limitations of thermal catalysis (Kim et al., 2016b). Plasmon-induced heating can be insignificant under low intensity exposures. Hot carriers can be transferred to adsorbate molecules through some kind of charge transfer. These reactions may include hot carrier injection to the molecular orbital of a targeted molecule, followed by coupling between plasmonic structures' excited electronic state and adsorbates. reaction pathways. (Fig. 2.6). In this way, specific and sometimes otherwise inaccessible reaction pathways can be activated (Chen, Zhu, Zhao, Zheng, & Gao, 2008; Naldoni et al., 2016).

Nanoplasmonics also has promising applications in photovoltaics (PVs) especially when used in conjunction with the conventional photovoltaic cells. The application is similar to the photocatalytic process in a way that it also requires hot carrier generation and carrier transfer. Conventional PV thin films are suffering efficiency issues due to

rapid recombination of electron/ hole pairs and high reflectance i.e poor absorption of light.

Also, many semiconductors have bandgap in the UV region, which make them unsuitable for almost 70-80% of solar spectrum absorbance which consists of visible to near infrared light. Plasmonic nanostructures can be very effective for *light trapping*, which will increase the light absorption of PVs (Atwater & Polman, 2010).

Additionally, hot carriers generated by plasmonic nanostructures can be transferred to the conduction band of semiconductors, which can increase the efficiency of the PVs (D. Liu et al., 2016; Wu, Chen, McBride, & Lian, 2015) . The electromagnetic enhancement in the LSPRs can increase the photocurrent of the PV's also (Dey & Zhao, 2016) (Fig. 2.7).



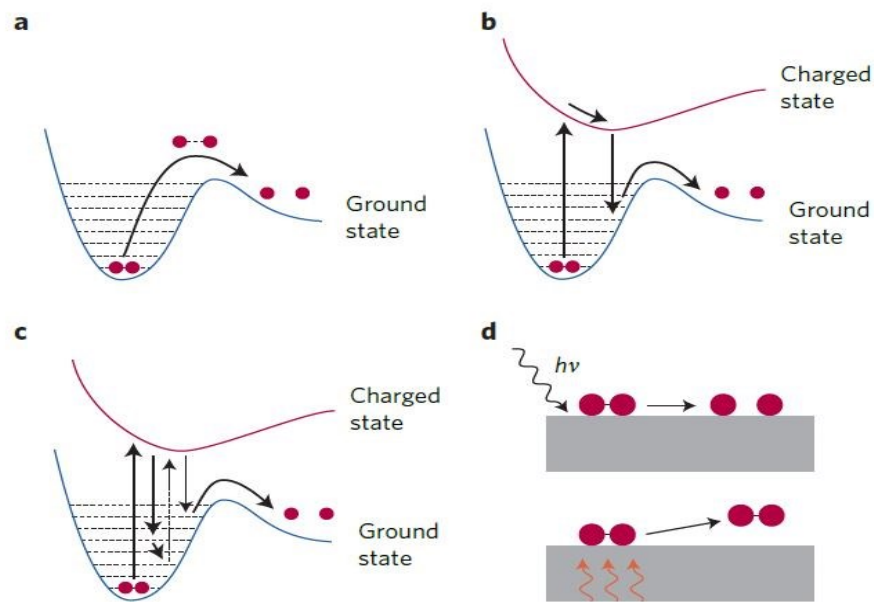


Fig. 2.6. (a) Di-atomic molecules are dissociated through thermal activation. (b) The dissociation of di-atomic molecules with the help of electrons. (c) When the incident flux of photon is high, electron can get injected in the di-atomic molecule before the molecular vibration is dissipated completely. (d) Plasmonic metal nanoparticles induce electron-driven reactions (top), which can trigger certain chemical reaction pathways that are not accessible otherwise (bottom). Reproduced with permission of Ref (Atwater & Polman, 2010).

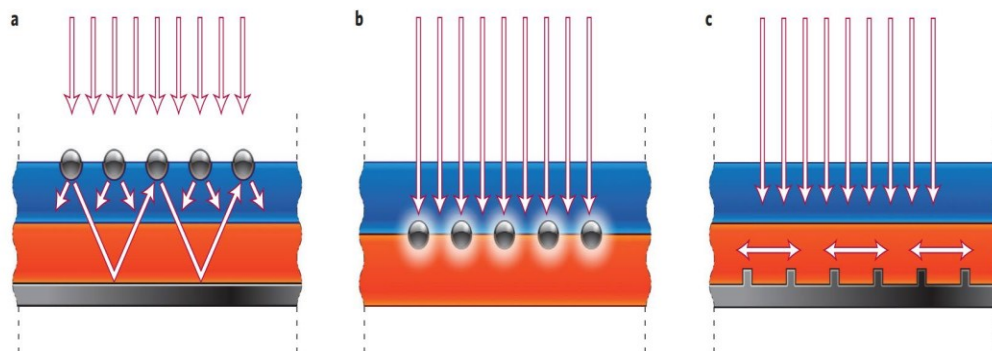


Fig. 2.7. Plasmonic light-trapping geometries for thin-film solar cells. (a) Light is trapped through scattering from metal nanoparticles at the surface of the solar cell. (b) Light can be trapped when it excites localized surface plasmons in metal nanoparticles embedded within the semiconductor. (c) When the excitation of surface plasmon polaritons occurs at the metal/semiconductor interface, light also is trapped. Reproduced with permission from Ref (Naldoni et al., 2016).

### CHAPTER THREE: OBJECTIVES

Importantly, the various functionalities of nanoplasmonics can be combined in a single platform. In this work, we attempted to induce chemical changes (reduction-oxidation) to a pigment, methylthioninium chloride or Methylene Blue (MB) by using nano-plasmonics, and to detect these changes by SERS in the same platform. The premier objectives of this work are as follows:

- Preparing and optimizing of Au coated nano- plasmonic substrates.
- Bio-funtionalizing of plasmonic substrates and immobilizing MB pigment from solution.
- Inducing chemical changes (reduction-oxidation) of immobilized MB pigment through plasmonic hot-spots, and detecting these changes by SERS in the same sample.

## CHAPTER FOUR: METHODS

In this section methods used in substrate preparation, bio-functionalization and characterization will be discussed.

### 4.1 Instruments Used for Plasmonic Substrate Fabrication and Characterization

The plasmonic substrates consist of noble metal nanostructures on dielectric supports because this enhances the surface plasmon resonance effect. Sputtering by ion bombardment is a very useful way to prepare metal nanostructures, as this is easy and effective. In the basic sputtering process, a target (or cathode) is bombarded by high-energy ions. The bombardment causes the removal of target atoms. These atoms fly in a vacuum chamber, resulting in a thin film deposited on a substrate. (Kelly & Arnell, 2000) A broadly used version of this process is known as magnetron sputtering. Magnetrons employ electric field configured such that ions from a plasma are directed towards a surface, whereas secondary electron motion is confined in the vicinity of the target. As a result the probability of ionization of a gas in the chamber through electron-atom collisions substantially increase, producing a dense plasma, which results in an increased bombardment at the target. This in turn results in a faster sputtering and, therefore, the rate of deposition at the substrate is high (Thornton, 1978). In our research, we used an Emitech K550X sputter coater from Quorum Technologies situated at Jordan Valley Innovation Center (JVIC). (Fig. 4.1.) It has the following features:

- Fully Automatic Control
- Low Voltage Sputtering

- High Resolution Fine Coating (Order of 2nm Gold Grain)



Fig. 4.1. Emitech K550X sputter coater from Quoram Technologies (Adapted with permission from Quoram Technologies).

Specification of Emitech K550X:

- Instrument Case 450mm Wide x 350mm Deep x 175mm High
- Work Chamber Borosilicate Glass 165mm Dia x 125mm High
- Safety Shield Polycarbonate
- Weight 18 Kg
- Target 60mm Dia x 0.1mm Thick (Gold fitted as Standard)
- Specimen Stage 60mm Dia. Rotating Stage with Tilt facility. (Spacing to Target 40mm)

- Vacuum Gauge Range ATM -  $1 \times 10^{-4}$  mbar
- Deposition Range 0-50mA
- Deposition Rate 0-25nm/Minute
- Sputter Timer 0-4 minutes
- Pre-set Needle Valve Control of Argon Supply

The atomic force microscope (AFM) system is a useful tool for direct measurements of micro-structural parameters and determining the intermolecular forces at nanoscale level with nanometric-resolution precision. Typically, AFM works on three modes; non-contact mode, contact mode, and tapping mode. The non-contact mode is utilized by moving the cantilever slightly away from the sample surface and oscillating the cantilever at or near its natural resonance frequency. It can probe electric, magnetic, and/or atomic forces of a selected sample. The contact mode acquires sample attributes by monitoring interaction forces while the cantilever tip remains in contact with the target sample. The tapping mode of operation combines qualities of both the contact and non-contact modes by gleaming sample data and oscillating the cantilever tip at or near its natural resonance frequency while allowing the cantilever tip to impact the target sample for a minimal amount of time. (Jalili & Laxminarayana, 2004; Meyer, 1992) In our research we have used a Bruker Dimension Icon AFM instrument of the Jordan Valley Innovation Center (JVIC). The instrument is equipped with a Nanoscope V controller, and operates in a tapping mode.

For cleaning of glass substrates, we used a sonicator and a plasma etcher. During sonication, the energy of sound waves is applied to clean the substrate. Usually ultrasonic (>20 KHz) sound frequencies are applied. These waves migrate through a medium

inducing pressure variations which in turn transforms the sound waves into mechanical energy. (Doktycz & Suslick, 1990) In our research we used a Bransonic 0.5 Gallon Ultrasonicator for substrate cleaning purposes. (Fig. 4.2.)



Fig. 4.2. Sonication bath.

We also used plasma etching to make sure there is no unwanted species on our substrate (Fig 4.3.). Plasma etching process uses a dense plasma consisting of electrons, ions, free radicals and molecules which constantly bombard the substrate. Depending on the gases that are used in forming the plasma, one can achieve both mechanical and

chemical cleaning.(Doktycz & Suslick, 1990) We used a RF plasma etcher of Jupiter III (Nordson March) instrument at JVIC with help of Rishi Patel to plasma etch our substrates.



Fig. 4.3. Plasma Etcher.

The Raman characterization was carried out with a Horiba LabRAM HR 800 Evolution Raman spectroscope. A 532 nm green laser was used for the Raman excitation, and the Stokes scattering was received with edge filter and detected by a CCD detector. The Edge filter blocks out and filters elastic Rayleigh scattering. The Band-pass filters

that are used in Raman pass only certain wavelengths and absorbs all other wavelengths. In this research, edge filter is used. Edge filters only let the Stokes scattered photons to pass. (Fig. 4.4).

The characterization parameters were optimized for Raman characterization of liquid samples. We used a 10X microscope lens for our focusing purpose of the samples (Fig. 4.5 and Fig. 4.6.). The photons that were able to make it through the edge filters (i.e. photons having larger wavelengths than the incident light) were passed through a 300 $\mu$ m confocal hole.



Fig. 4.4. Horiba LabRAM HR 800 Evolution Raman spectrometer



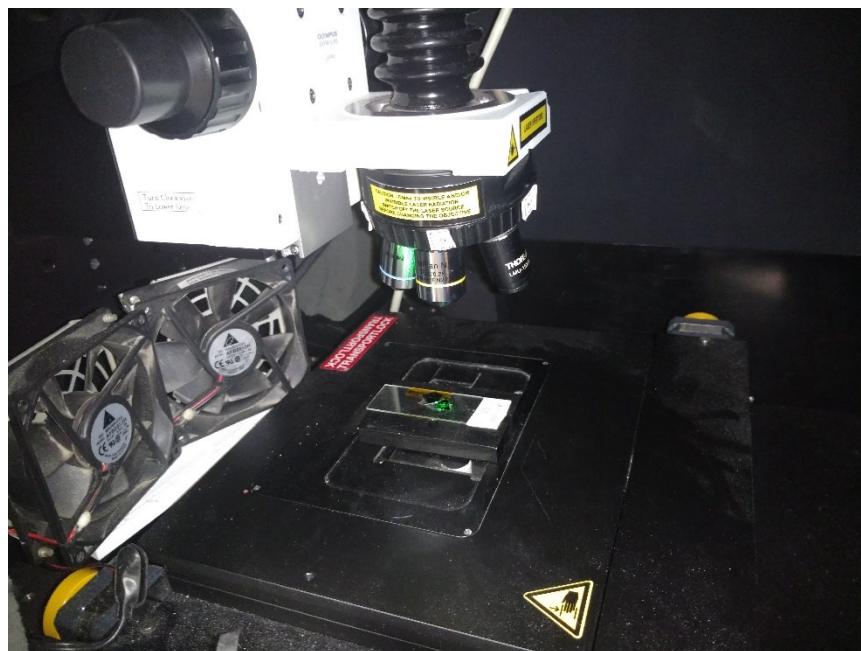


Fig. 4.5. Raman spectroscopy setup: A 10x microscope is exposing 532 nm laser on a substrate.

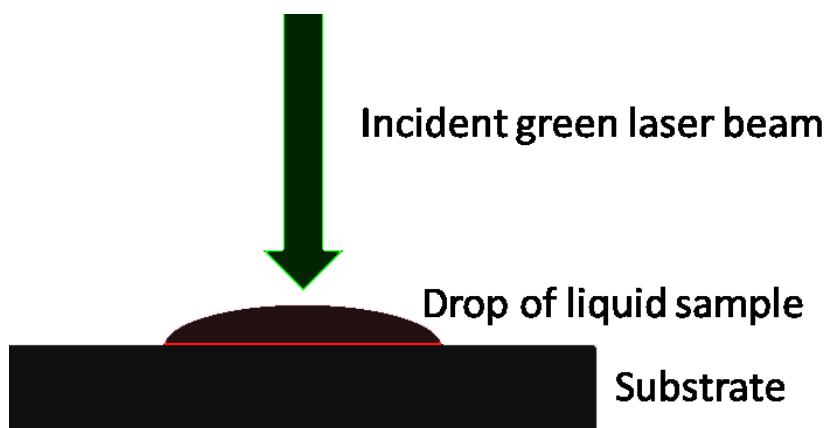


Fig. 4.6. Schematic of the experimental setup of Raman spectroscopy of liquid Samples.

We used a Laser Quantum Torus 532nm Green laser with a mpc3000 power source with 50mW laser power as our laser source Fig 4.7. The detailed specifications of the Torus laser are listed below:

Wavelength	532 nm
Beam Size	1.7 mm $\pm$ 0.2mm
Bandwidth	1 MHz
Power stability	< 1.0% RMS
RMS noise	< 0.5%
Noise bandwidth	1Hz - 100MHz
Coherence length	> 100m
Operating temperature	15 - 35° C
Head weight	1.2 kg
Warm-up time	<30 mins



Fig. 4.7. Taurus mpc3000 532nm Green lase by Laser Quantum.

NGS LabSpec 5 software was used to display and store the data. To analyze the Raman spectra, background subtraction was done by the OriginPro 8.5.1 software. Prior to this Raman data were saved as a .txt file using LabSpec 5. Background subtraction was performed using a 4<sup>th</sup> order polynomial interpolation. The Raman spectrometer was calibrated by using a standard silicon wafer regularly.

## 4.2 Instruments and Chemicals Used for Biofunctionalization

We used Tris-EDTA buffer solution from Sigma Aldrich. (Fig.4.8). It is a common buffer solution that is used to solubilize DNA and RNA without degrading them (Yagi et al., 1996).

Sulfur is attached to Au by chemisorption. DNA can be attached to Au surfaces by mediation of sulfur (thiol) groups (Pensa et al., 2012). The thiol-Au bond is very strong (40/50 kcal/mole). We purchased lyophilized thiolated single stranded DNAs 5'-GGTTTGGAGGGGC CA-3' from Sigma Aldrich for bio-funtionalization of our Au coated glass substrates.(Pensa et al., 2012)

A pH meter is employed to measure the alkalinity and basicity of a solution. In this research we used a calibrated standard pH meter to monitor the pH of Tris-EDTA buffer and DNA solutions. A Vortex mixer from Fisher Scientific was used to make the DNA solution. Micropipette was used to transfer the small amounts of solutions.

As our target analyte we used Methylthioninium Chloride popularly known as Methylene Blue (MB). Molecular formula of Methylene Blue is  $C_{16}H_{18}ClN_3S$  . Methylene Blue is a very common oxidation-reduction indicator. In its oxidized state it is blue in color and in reduced state it is colorless. This reduced state is known as Leucomethylene Blue and has a molecular formula  $C_{16}H_{19}N_3S$  .We purchased a 1.5% solution of Methylene Blue from Sigma Aldrich for our research. We used HPLC grade water from Thermo Fisher to dilute some of the solutions. (Fig. 4.8).

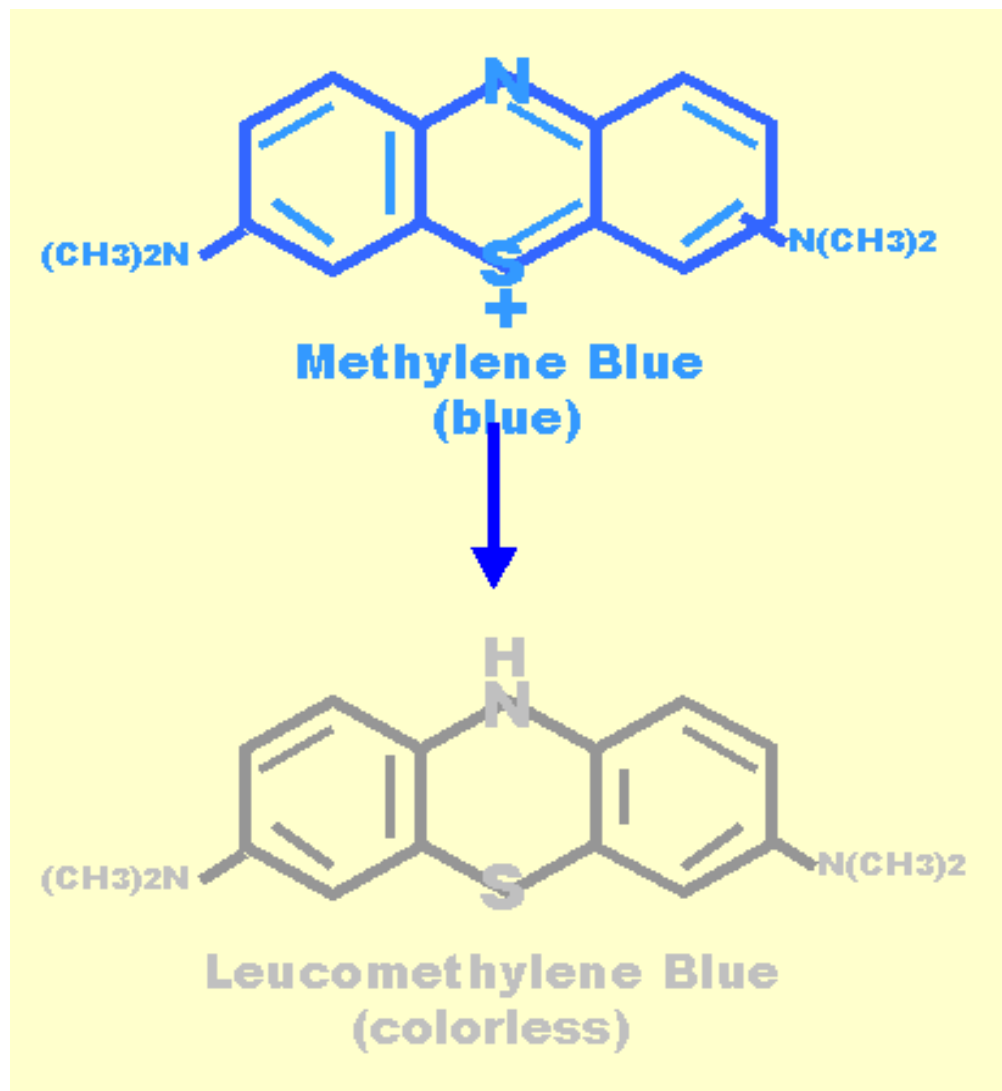


Fig. 4.8. Oxidized (top) and reduced (bottom) structures of methylene blue. Reproduced with permission from Ref. <sup>50</sup>.

The solutions were preserved in test tubes purchased from Sigma Aldrich. The glass slides that we used for Au coated glass substrate were purchased from Thermo-Fisher Scientific. A medical grade refrigerator was used for the incubation purpose.

## CHAPTER FIVE: RESULTS

### 5.1 Protocols Used to Fabricate Nano-Bio Conjugate System

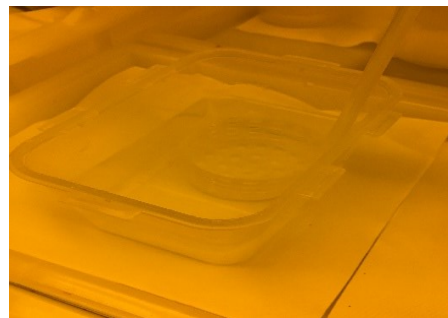
Plasmonic nanostructures were created by magnetron deposition of thin gold coating on glass substrates using a sputter system with a deposition rate of 10 nm/min. Prior to the Au coating, a thorough cleaning of glass substrates was done. The glass substrates were first washed with acetone and DI water; then they were taken to sonication bath for acetone sonication for 5 min. After the sonication, each sample was nitrogen-dried. Finally, the substrates were RF plasma-etched. Etching was performed for 1 min with a mixture of Ar and H<sub>2</sub> followed by 30 sec of H<sub>2</sub> etching (Fig. 5.1.).

We have employed the Atomic Force Microscopy (AFM) to characterize our gold coated glass samples. The atomic force microscopy results show surface morphology and roughness of gold coated glass substrates at varying thickness of coating. (5nm, 10nm, 15nm, 20nm, 25nm & 30nm) (Fig. 5.2. & Fig.5.3.). From these figures we can observe that the sputter deposition of Au creates random islands of Au nano-structures. The surface area of an individual nano-structure increases with the increased deposition time. The distance between any two nanostructures decreases with increased deposition thickness. A 5nm thickness coating has the highest relative roughness followed by 10nm, 15nm, 20nm, 25nm and 30nm, which has the least relative roughness.

By comparing the results of roughness, nanostructure surface area and distance between adjacent nano-structures, we identified 15 nm as our desired thickness of Au coating on glass to function as our plasmonic nanostructure.



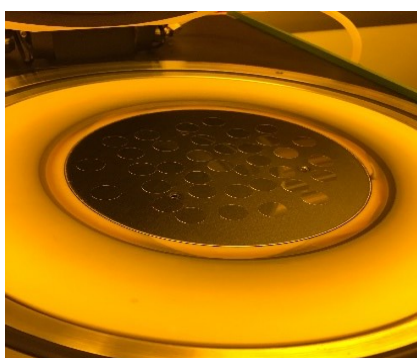
2% H<sub>2</sub>SO<sub>4</sub> cleaning solution



5 min dipping in cleaning solution



Acetone sonication for 5 mins.



Clean slides placed on a plasma cleaning platform



Sputtering carried out by fixing up parameters that ensures a 10 nm/min deposition



1 min Ar+O<sub>2</sub> plasma cleaning followed by a 30 sec Ar cleaning only

Fig. 5.1. Au coated glass substrate preparation steps.

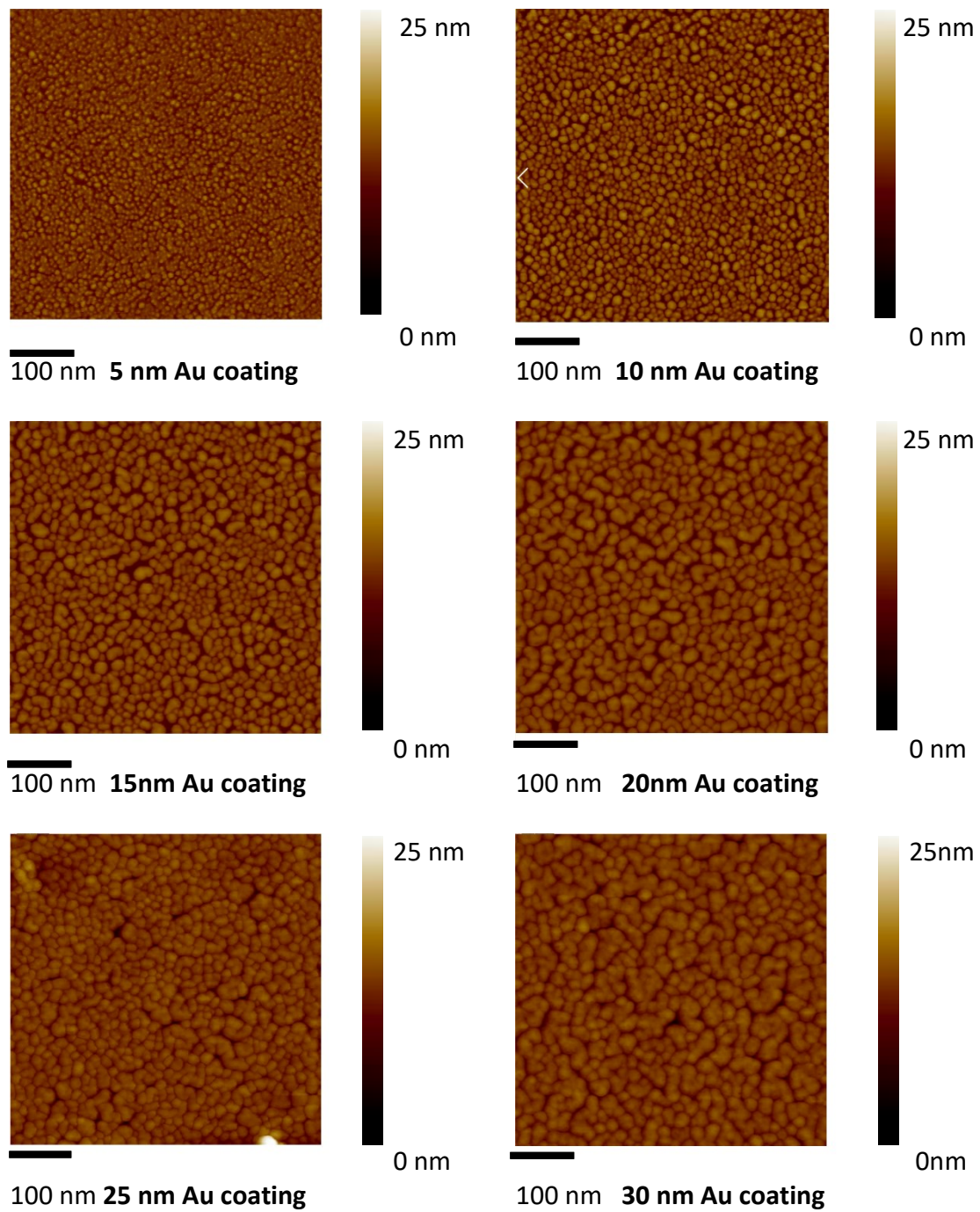


Fig. 5.2. AFM surface morphology of Au coated glass substrates at different coating thickness (5nm -30nm).



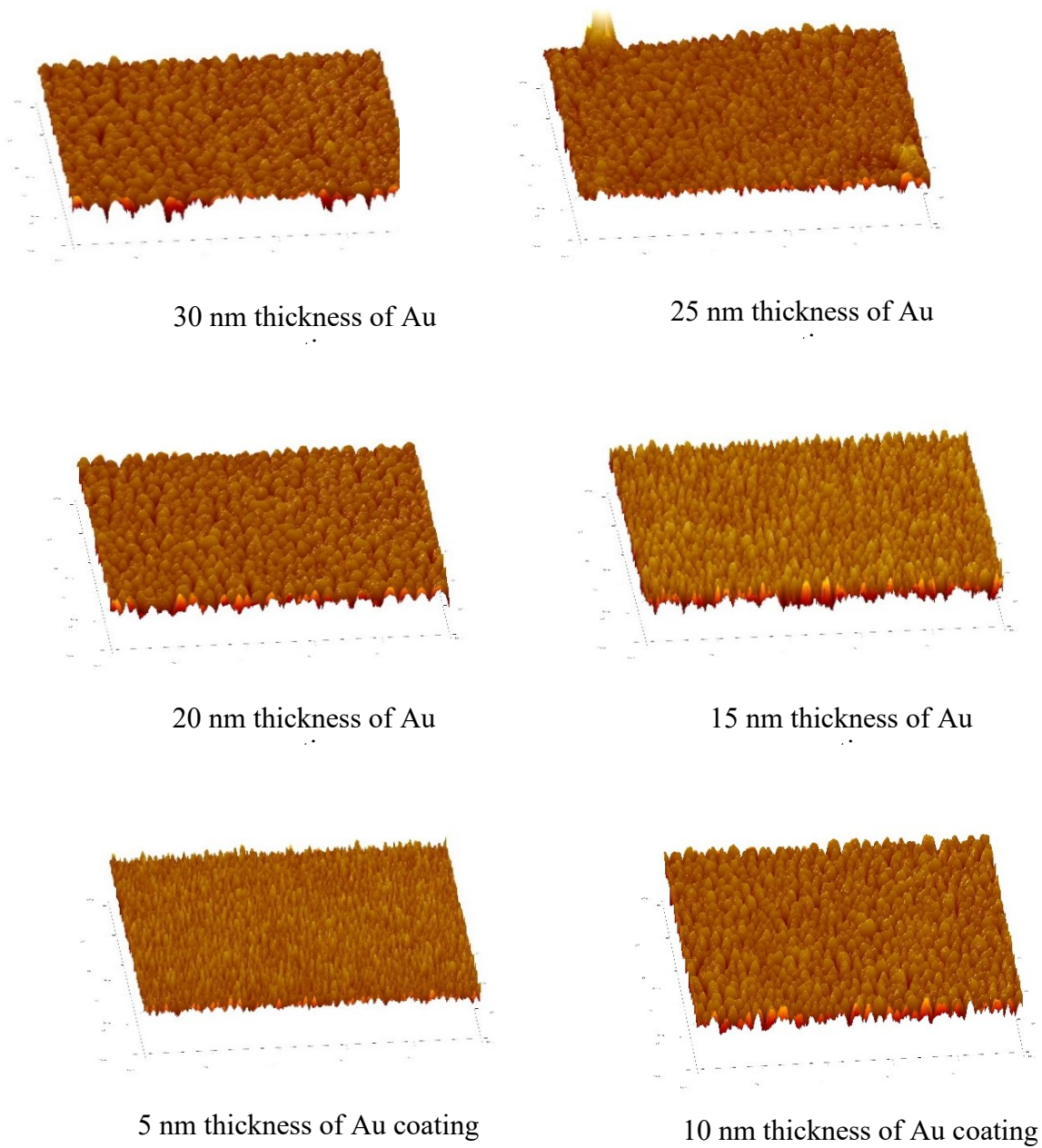


Fig. 5.3. AFM 3-D topographical image of Au coated glass substrates at different coating thickness.

After cleaning and Au deposition, the substrates were biofunctionalized as schematically shown in Fig. 5.4. For this purpose, thiolated DNA strands 5'-GGTTTGGAGGGGC CA-3' were used. An 1  $\mu$ M DNA solution was prepared with Tris-EDTA buffer at a pH of 7. The DNA solution was kept at 5°C. To biofunctionalize the samples, a 100  $\mu$ l drop of DNA solution was deposited onto the gold-coated substrates. Next, a 100  $\mu$ l drop of the MB solution (4.7 mM, Sigma-Aldrich) was added onto the same spot, and the samples were incubated for 24 h at 5°C. The incubation was done in humid environment to avoid drying of the samples. For this purposes, a two-compartment Petri dish was used. The sample was placed in one compartment, and second compartment contained DI water. Fig. 5.5. illustrates the functionalization process.

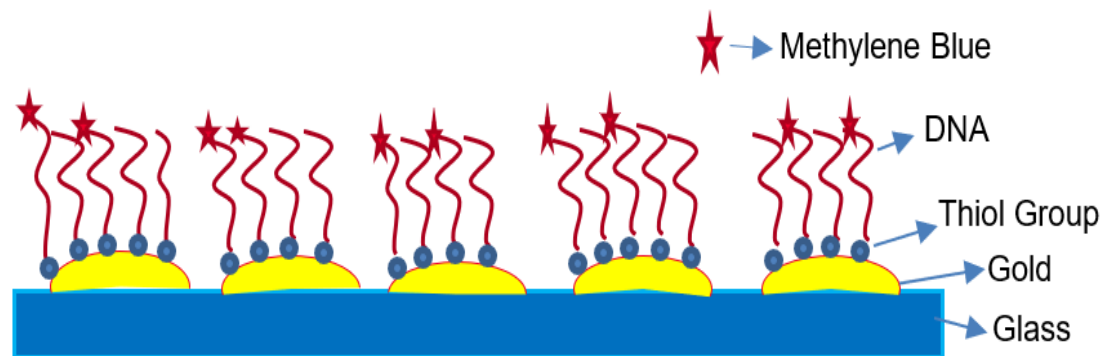


Fig. 5.4. Scheme of DNA functionalized, gold-coated plasmonic substrate.

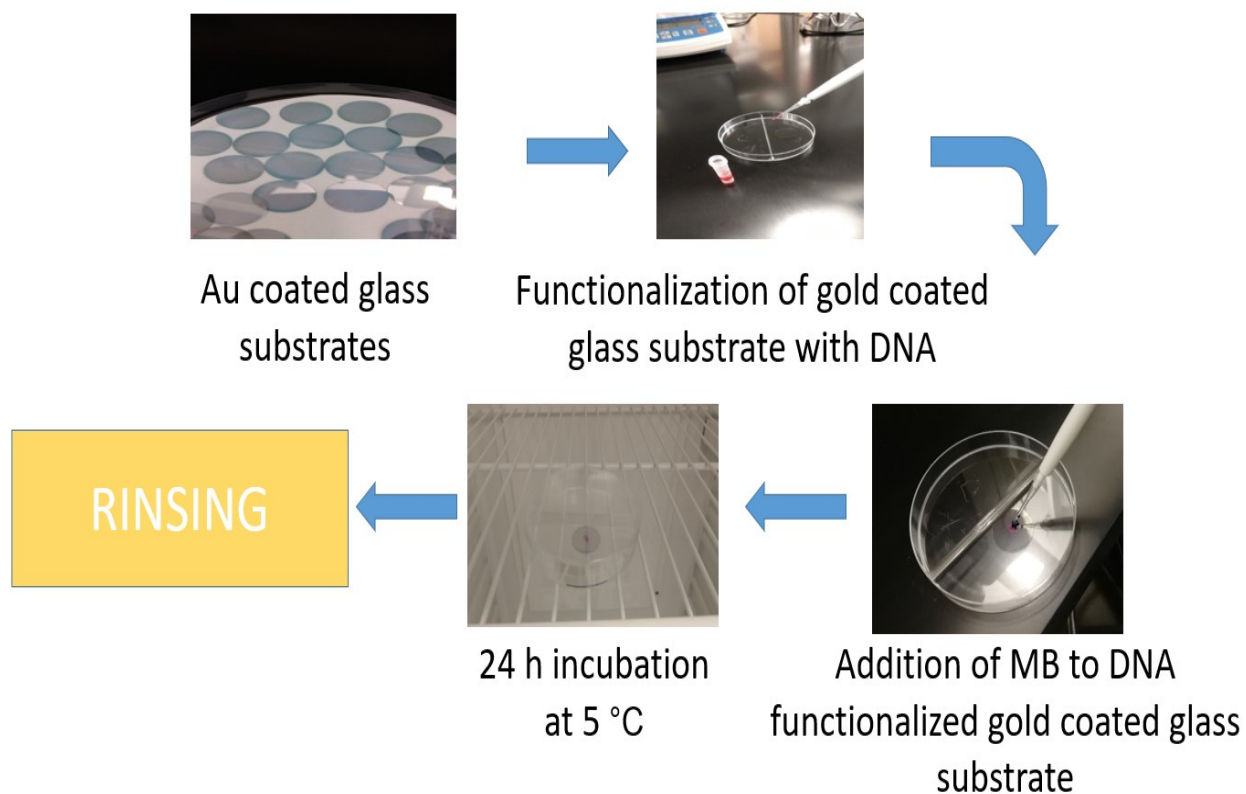


Fig. 5.5. Steps of substrate bio-functionalization with DNA and methylene blue.

It has been expected that during incubation, DNA strands attach to the gold coating through the thiol groups (Pensa et al., 2012), whereas MB binds to guanine bases of DNA (Vardevanyan, Antonyan, Parsadanyan, Shahinyan, & Hambardzumyan, 2013). For comparison, control samples were also prepared by incubating similar gold-coated glass substrates with the MB solution alone in the absence of DNA (Fig.5.4.).

## 5.2 Benchmark Raman and SERS Characterization of All Components

Fig.5.6 and Fig.5.7. show the benchmark Raman spectra of Tris-EDTA buffer, DNA solution on Gold coated glass substrates. These two are not Raman active, which is evident from their respective Raman spectra.

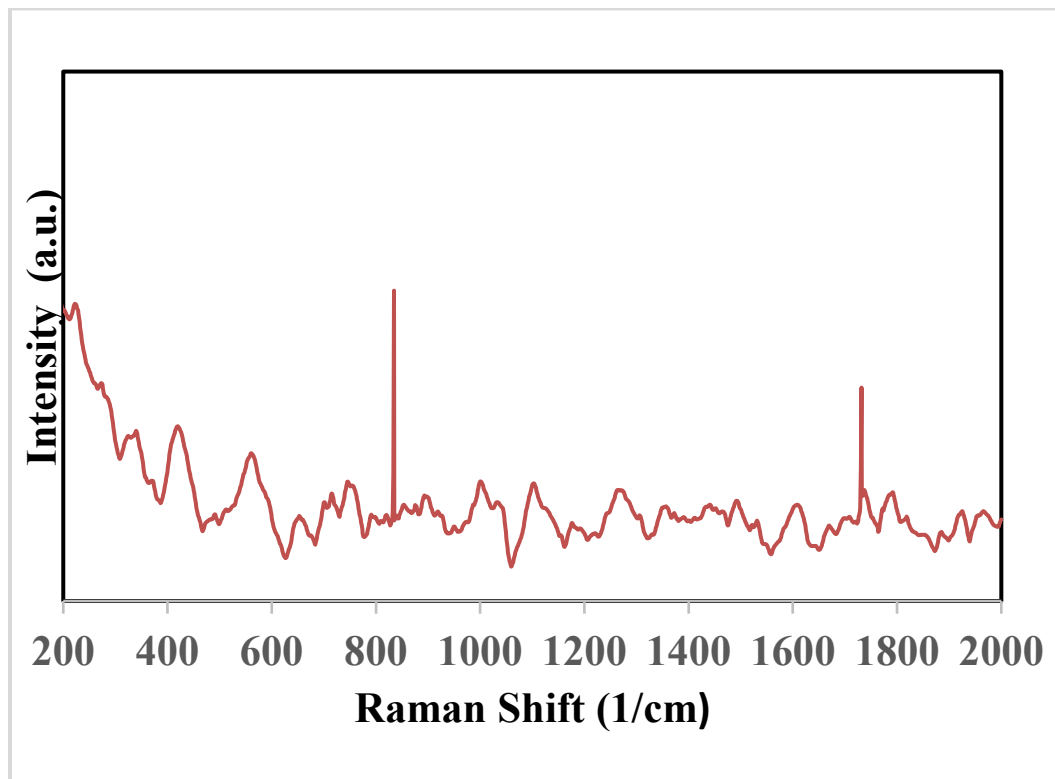


Fig. 5.6. Benchmark Raman spectrum of Tris-EDTA buffer on Au coated glass substrate. No characteristic peaks observed.

Fig. 5.8. Shows a typical benchmark Raman spectrum of methylene blue solution. To prepare this sample, a 100  $\mu\text{L}$  drop of the MB solution was deposited onto a gold-coated glass slide, and Raman characterization was performed immediately without incubation or rinsing. The spectrum exhibits pronounced bands that we have attributed to stretching of C=C bond of MB's aromatic ring at  $1625\text{ cm}^{-1}$ ; vibrations of C=N bonds

and CH<sub>3</sub> groups between 1398 cm<sup>-1</sup> and 1470 cm<sup>-1</sup>; and C-N-C skeletal bending at 501 cm<sup>-1</sup> and 446 cm<sup>-1</sup> (Nicolai & Rubim, 2003; Xiao & Man, 2007).

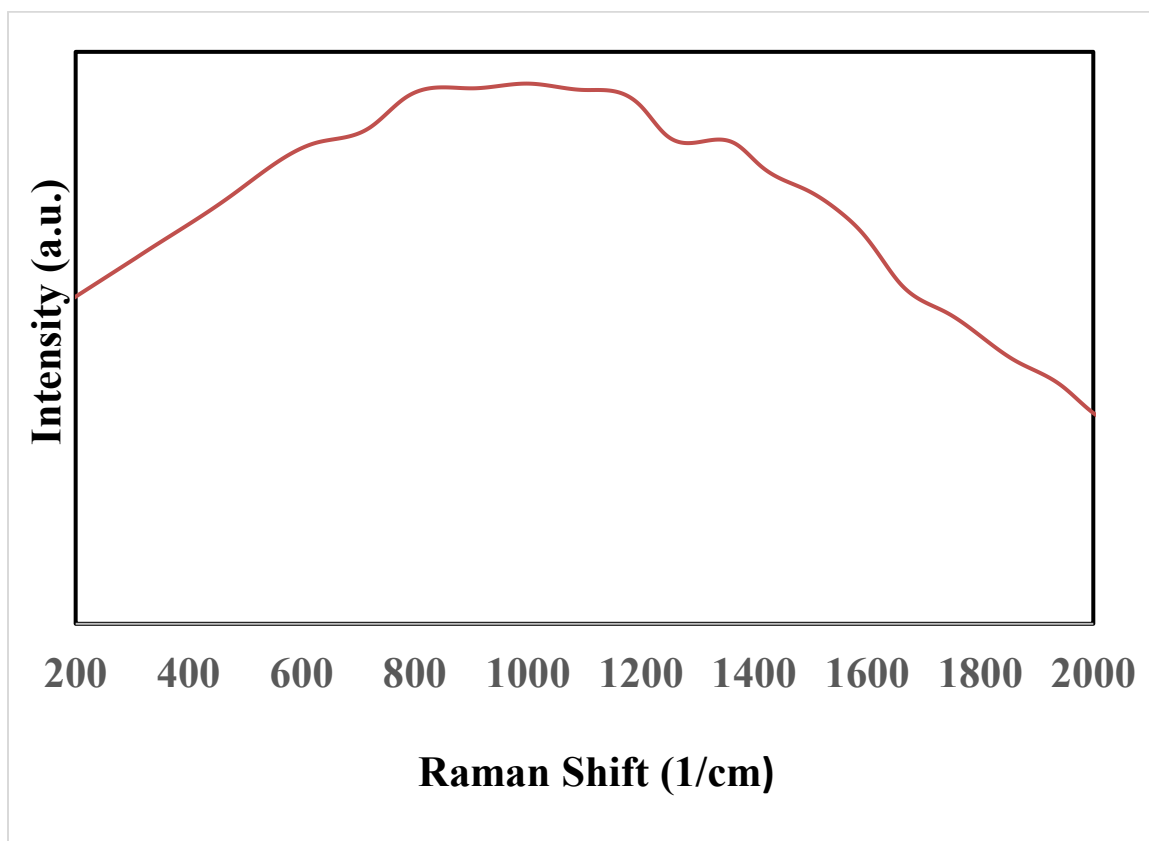


Fig. 5.7. Raman spectrum of ss-DNA incubated on gold coated glass slide.

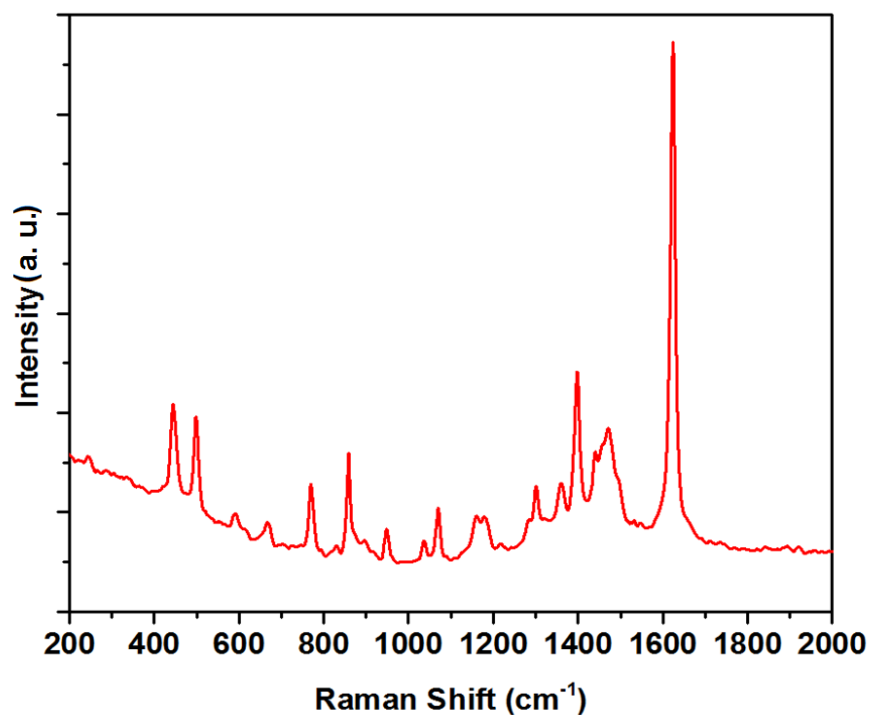


Fig. 5.8. Raman spectrum of methylene blue solution on gold coated glass substrate without incubation

Next, the same amount of MB solution was incubated on gold-coated glass substrates for 24h at 5°C. Then, the samples were rinsed in the Tris-EDTA buffer and their Raman spectra collected. An example spectrum is shown in (Fig. 5.9). It can be seen that in the absence of DNA functionalization, the spectrum does not exhibit Raman bands characteristic of MB. After rinsing the Methylene-Blue gets rinsed off the Au coated glass surface.

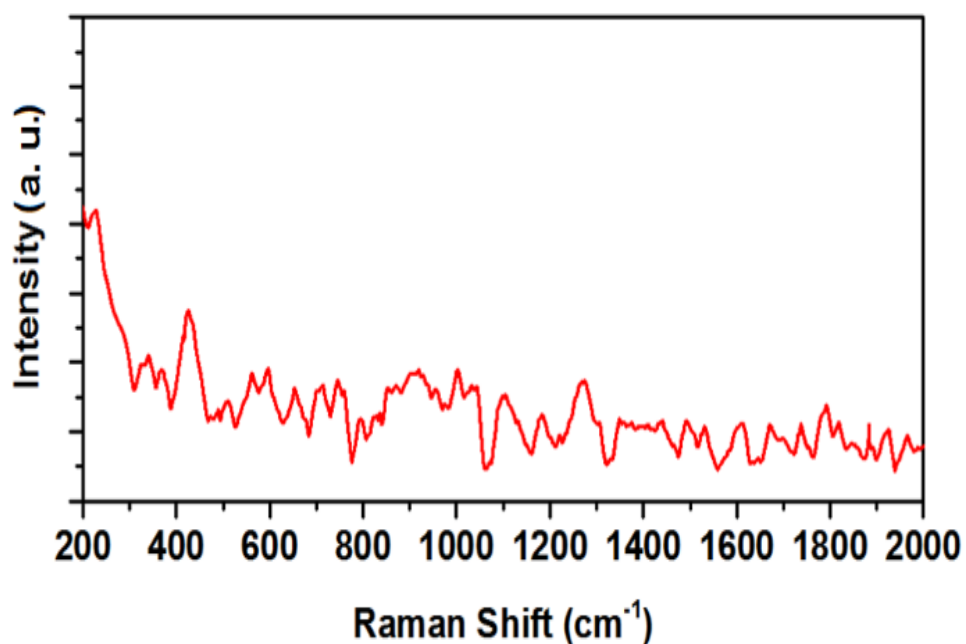


Fig. 5.9. Raman spectrum of rinsed gold-coated glass substrate after a 24 h incubation with methylene blue in the absence of DNA functionalization.

### 5.3 SERS Detection of Reduction-Oxidation Processes Stimulated by LSPR Hot-Spots under Laser Excitation

Fig. 5.10. shows a SERS spectrum of DNA-functionalized substrate incubated with the addition of MB. In striking contrast with DNA-free experiments., When the Au coated glass substrate is bio-functionalized with the DNA, pronounced Raman bands of methylene blue are visible after rinsing. These include a strong peak at approximately  $1623\text{ cm}^{-1}$ .

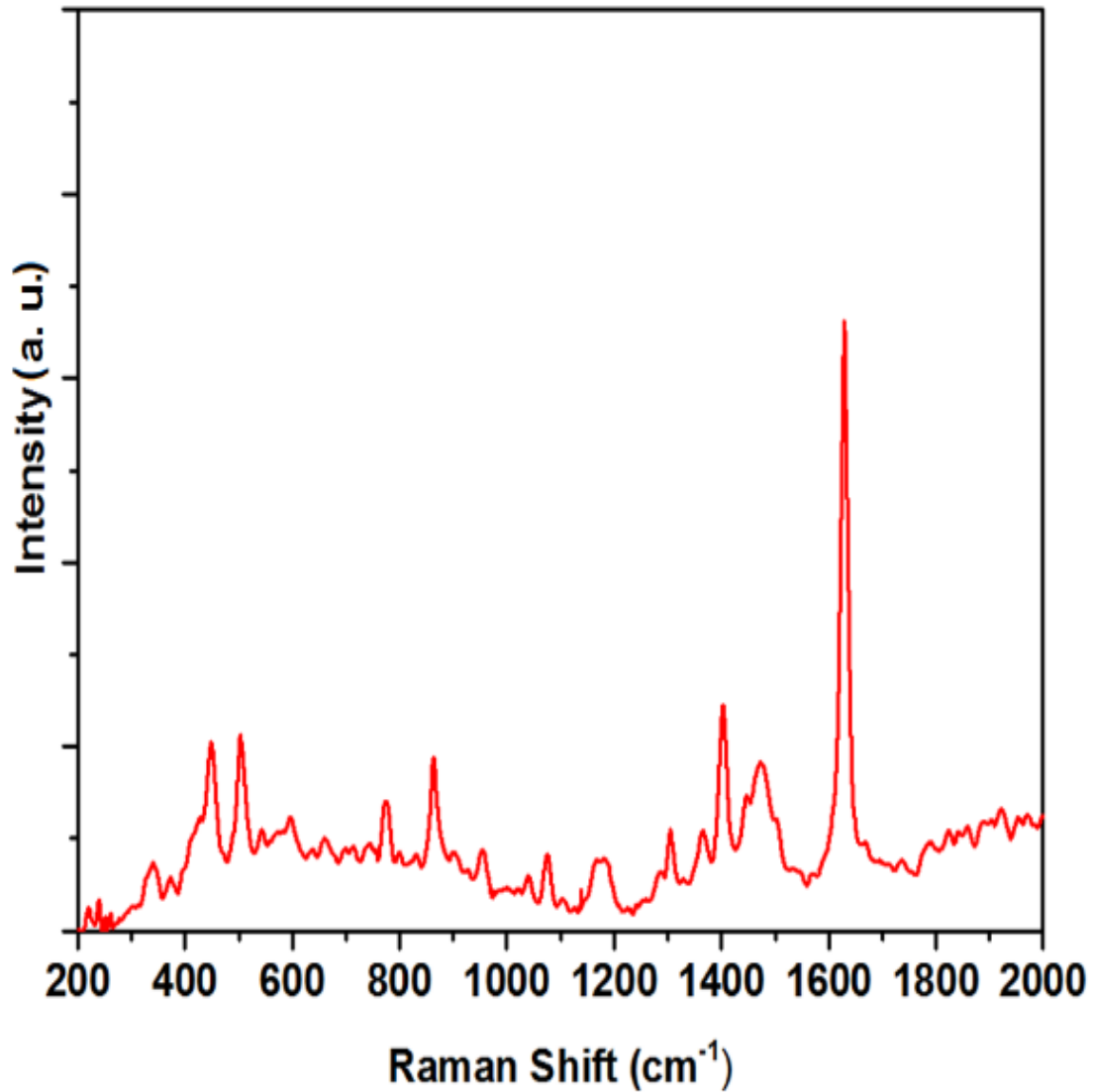


Fig. 5.10. SERS spectrum of DNA-functionalized, MB-loaded gold coated glass substrate after a 24 h incubation and rinsing.

Next, we have investigated the evolution of SERS spectra of DNA-functionalized and MB-loaded samples after 20 min, 40 min, 60 min, 80 min, 100 min, 120 min, and



140 min of exposure to a 523 nm laser excitation. As it can be seen from Fig 5.11, the Raman bands have decayed with time. After 100 min of exposure to the laser, Raman fingerprint of MB has completely disappeared. Then, we added 20  $\mu\text{L}$  of Tris-EDTA buffer (pH 7) on the same substrate, and continued the laser exposure. Remarkably, this resulted in a recovery of MB's Raman fingerprint. After 160 min, pronounced Raman bands at  $1626\text{ cm}^{-1}$  and  $1396\text{ cm}^{-1}$  characteristic of MB have been detected again.

Continuing the exposure beyond this point caused the Raman bands disappearing and reappearing again, in a similar reversible fashion. To further investigate this phenomenon we carried out the experiment for a longer period of time and we could see repetitive reduction-oxidation cycles (Fig 5.12.)

For the sake of comparison, we also have deposited a  $0.5\text{ }\mu\text{L}$  drop of the MB solution onto a cleaned glass slide without gold coating and DNA functionalization. This control sample was immediately exposed to the 532 nm laser excitation, and the entire experiment was repeated as described above. As Fig. 5.13. illustrates, in this case a characteristic Raman band, centered at approximately  $1629\text{ cm}^{-1}$ , has remained after 100 min of exposure. Subsequent addition of  $20\text{ }\mu\text{L}$  of Tris-EDTA buffer did not change the Raman fingerprint.

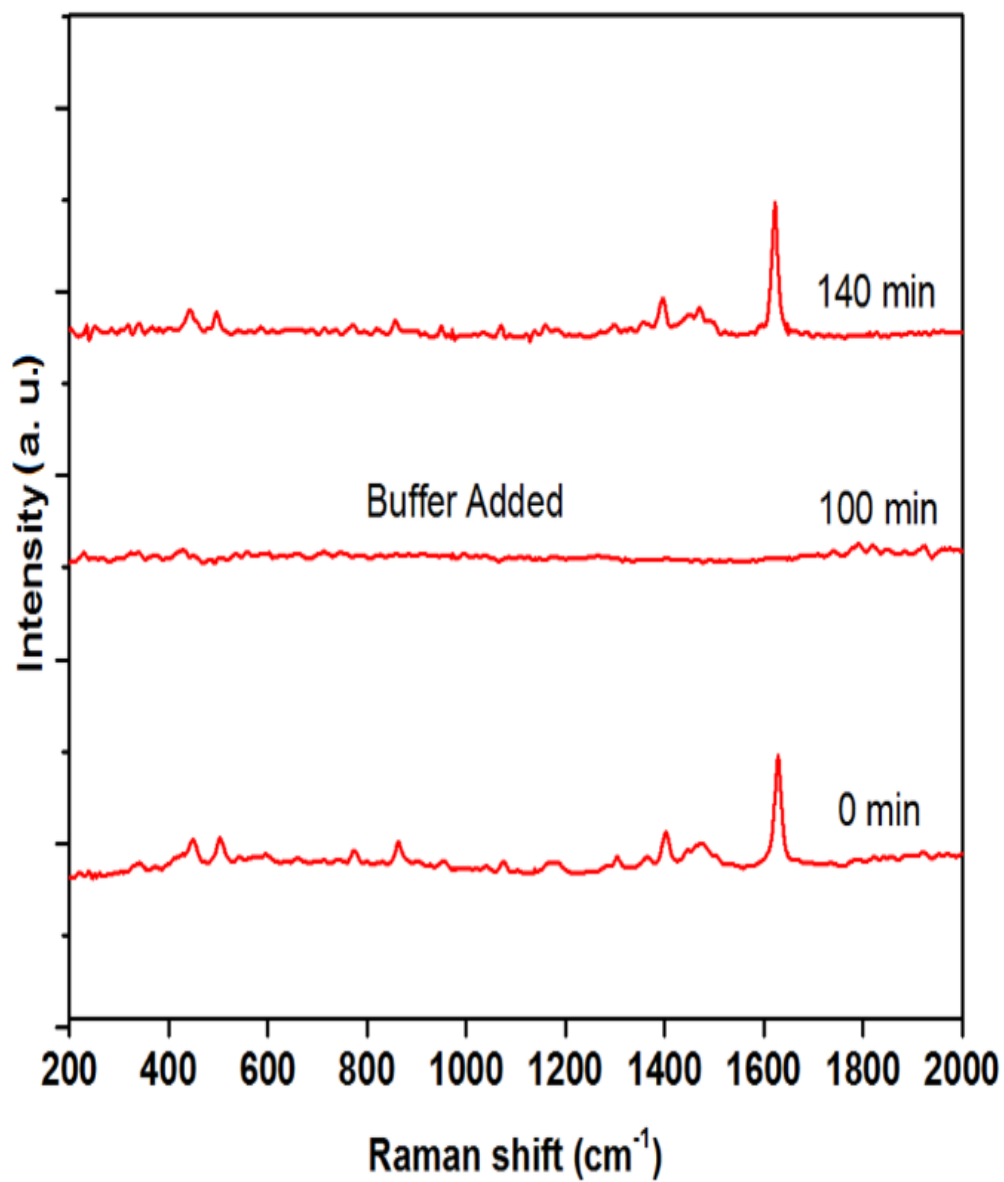


Fig. 5.11. SERS spectra of DNA-functionalized, MB-loaded gold-coated glass substrate at the beginning of a 523 nm laser exposure (bottom); after 100 min of the exposure (middle); and after 140 min of the exposure following the addition of Tris-EDTA buffer (top). A vertical offset was applied to the spectra for clearer presentation.

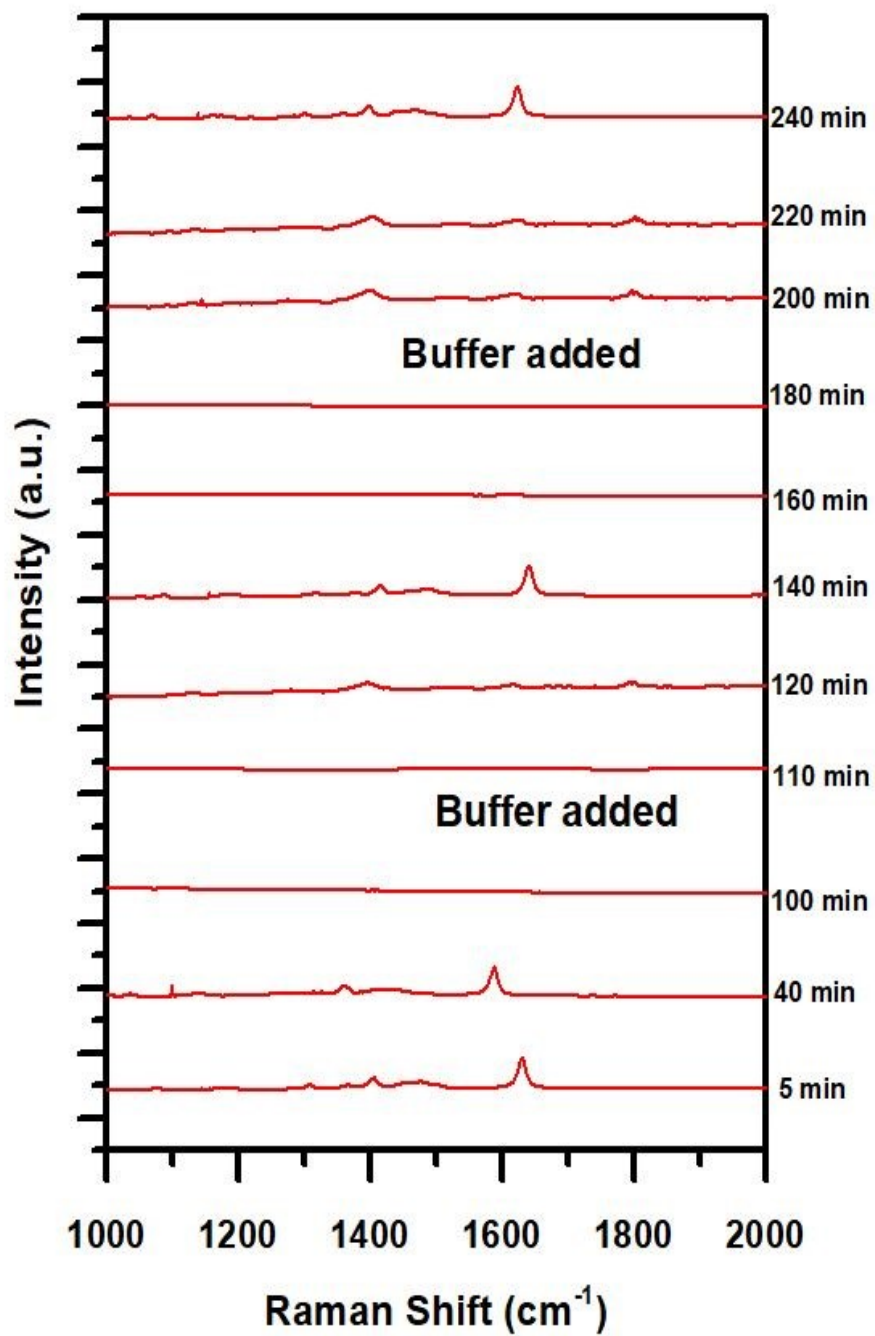


Fig. 5.12. Reduction-oxidation cycle of Methylene blue at neutral pH and in absence of electrode potential on Au coated glass plasmonic substrates.

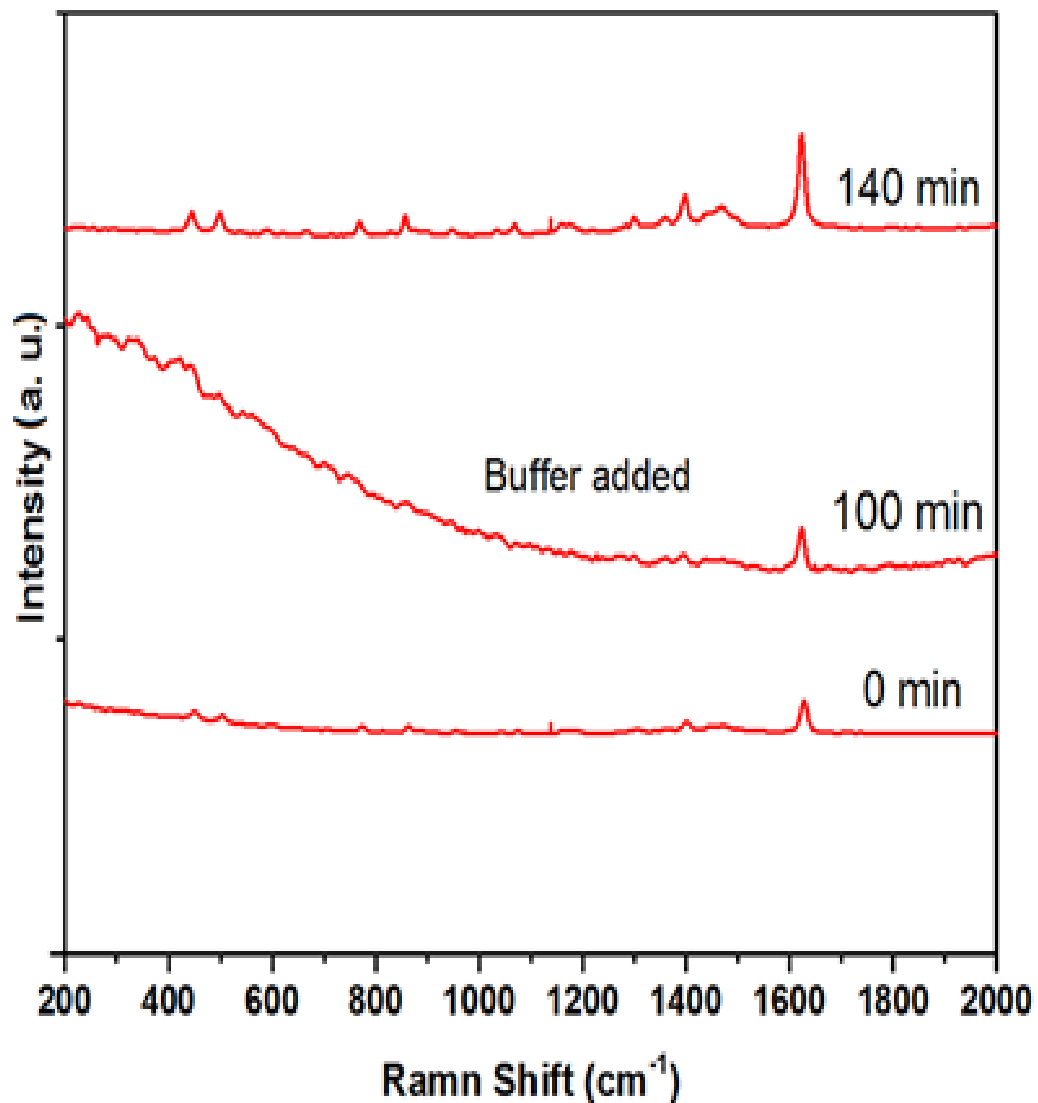


Fig. 5.13. Raman spectra of a drop of MB solution on a bare uncoated glass slide at the beginning of laser exposure (bottom); after 100 min of the exposure (middle); and after 140 min of the exposure following the addition of Tris-EDTA buffer (top). A vertical offset was applied to the spectra for clearer presentation.

## CHAPTER SIX : DISCUSSIONS

The results presented in Figs. 5.9 and 5.10 indicate that in the absence of DNA functionalization, methylene blue does not attach to gold-coated substrates strongly enough to remain on the surface after rinsing. However in the presence of DNA, pronounced SERS signal of MB indicates its presence on the surface after rinsing. We expect that during the incubation, DNA binds to the surface of gold through the mediation of thiol groups (Pensa et al., 2012) , whereas MB binds to guanine bases of DNA (Vardevanyan et al., 2013), which plays a role of surface-immobilized linker.

Remarkably, after rinsing of the incubated samples, MB-loaded, surface-immobilized DNA is supposed to be present in a monolayer quantity or less. Therefore, pronounced Raman fingerprints such as shown in Fig. 5.10 correspond to a very small quantity of MB molecules, indicating significant SERS enhancement in our samples.

A well-known redox indicator, MB can adopt oxidized or reduced forms, which differ in charge and protonation state(Farjami, Clima, Gothelf, & Ferapontova, 2010). In water or buffer solution at neutral or acidic pH conditions MB would adopt an oxidized form, which produces a characteristic Raman spectrum such as shown in Fig. 5.8. As our results indicate, similar fingerprints are also observed in SERS spectra from MB-loaded, substrate-immobilized DNA after relatively short exposures to laser excitation (Figs. 5.10, 5.11 and 5.12). However, more extensive exposures to the laser light in the presence of the buffer have resulted in disappearance of the Raman fingerprint (Fig.5.11).

Degradation of Raman bands of MB can be attributed to its reduction, as it was demonstrated by electrochemical stimulation of DNA-bound MB (Papadopoulou et al., 2016). In this published work (Papadopoulou et al., 2016), double stranded DNA loaded

with methylene blue was immobilized on gold electrodes. Incubated overnight and MB pigments were immobilized after the incubation. The changed electrode potential was changed from 0 mV to -500 mV at a rate of 0.7mV/s. This resulted in a gradual decrease of the Raman bands with the applied potential (Fig. 5.14(a)). In particular, the peaks at  $1622\text{ cm}^{-1}$  and  $1388\text{ cm}^{-1}$  which correspond to the aromatic C=C and C=N ring stretches, have decreased with height and eventually disappeared completely at  $\sim -500\text{mV}$ . When the potential is reversed from -500mV to 0mV, the Raman peaks reappeared. (Fig. 5.14 (b)). Based on these results, disappearance of MB's characteristic Raman bands can be indicative of its reduction, and vice versa.

Therefore, we expect that the changes of Raman Spectra that we observe indicate reduction of MB, followed by oxidation. Importantly, in our work, the observed reversible reduction-oxidation transformations of MB occurred at neutral pH in the absence of electrodes or chemical agents other than the buffer. However, the presence of gold coating has been critical for these transformations. As Fig. 5.13 indicates, exposure to laser excitation did not induce a reduction of MB solution on a bare un-coated glass slide. From 5.12. we conclude that this reversible reduction-oxidation cycle can be repetitive during prolonged laser exposure and with the addition of buffer solution. We hypothesize that energy of plasmonic hot-spots generated by laser excitation in the gold coating is required for the reversible transformation of MB to occur.

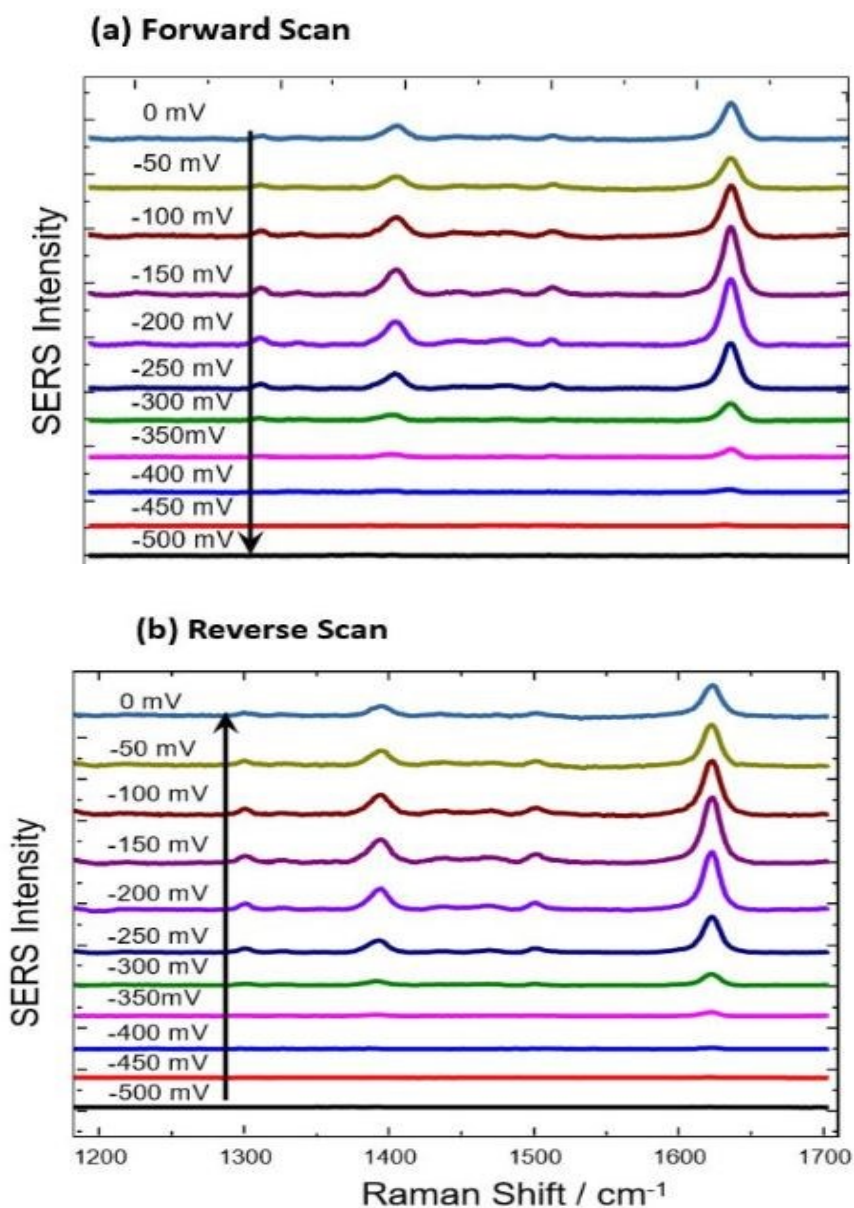


Fig. 5.14. Raman spectra demonstrating electrochemically-driven reduction-oxidation of MB. Reduction of MB : (a) With increasing negative electrode potential, the characteristic peaks of MB dies down and disappears at  $\sim -500$  mV. Oxidation of MB: (b) When the potential is reversed the characteristic peaks starts reappearing. Reproduced with permission from Ref (Papadopoulou et al., 2016)- Published by The Royal Society of Chemistry.

## CHAPTER SEVEN: CONCLUSIONS

In this work, multi-functional application of nanoplasmonics has been demonstrated. This includes inducing chemical changes into a material immobilized on a plasmonic substrate, and detection of these changes using SERS within the same experimental platform. In particular:

- Plasmonic substrates comprising gold nanostructures on glass were fabricated and characterized;
- A process of functionalization of the substrates by DNA carrying an important reduction-oxidation indicator methylene blue, was developed;
- Immobilized, DNA-bound MB was detected by SERS in submonolayer quantities;
- Reduction-oxidation of MB at neutral pH was detected in the same design;
- These chemical changes are attributable to the influence of plasmonic ‘hot-spots’ under laser excitation in the presence of the buffer.

The results of this research can be useful for many other systems, in particular, this research work has paved the way to the further investigation of plasmonic photocatalysis.

Future research may include:

1. Theoretical study of the reversible reduction-oxidation of MB in this system at neutral pH.
2. Development of bio functionalization processes of plasmonic substrates to immobilize different materials.



3. Building models that can simulate plasmonic photocatalysis in various designs.

## REFERENCES

- Anker, J. N., Hall, W. P., Lyandres, O., Shah, N. C., Zhao, J., & Van Duyne, R. P. (2008a). Biosensing with plasmonic nanosensors. *Nature Materials*, 7(6), 442–453. <https://doi.org/10.1038/nmat2162>
- Anker, J. N., Hall, W. P., Lyandres, O., Shah, N. C., Zhao, J., & Van Duyne, R. P. (2008b). Biosensing with plasmonic nanosensors. *Nature Materials*, 7(6), 442–453. <https://doi.org/10.1038/nmat2162>
- Atwater, H. A., & Polman, A. (2010). Plasmonics for improved photovoltaic devices. *Nature Materials*, 9(3), 205–213. <https://doi.org/10.1038/nmat2629>
- Bantz, K. C., Meyer, A. F., Wittenberg, N. J., Im, H., Kurtuluş, O., Lee, S. H., ... Haynes, C. L. (2011a). Recent progress in SERS biosensing. *Physical Chemistry Chemical Physics : PCCP*, 13(24), 11551–11567. <https://doi.org/10.1039/c0cp01841d>
- Bantz, K. C., Meyer, A. F., Wittenberg, N. J., Im, H., Kurtuluş, Ö., Lee, S. H., ... Haynes, C. L. (2011b). Recent progress in SERS biosensing. *Physical Chemistry Chemical Physics*, 13(24), 11551. <https://doi.org/10.1039/c0cp01841d>
- Barnes, W. L., Dereux, A., & Ebbesen, T. W. (2003). Surface plasmon subwavelength optics. *Nature*, 424(6950), 824–830. <https://doi.org/10.1038/nature01937>
- Brosseau, C. L., Casadio, F., & Van Duyne, R. P. (2011). Revealing the invisible: using surface-enhanced Raman spectroscopy to identify minute remnants of color in Winslow Homer's colorless skies. *Journal of Raman Spectroscopy*, 42(6), 1305–1310. <https://doi.org/10.1002/jrs.2877>
- Cao, Y. C., Jin, R., & Mirkin, C. A. (2002a). Nanoparticles with Raman spectroscopic fingerprints for DNA and RNA detection. *Science (New York, N.Y.)*, 297(5586), 1536–1540. <https://doi.org/10.1126/science.297.5586.1536>
- Cao, Y. C., Jin, R., & Mirkin, C. A. (2002b). Nanoparticles with Raman Spectroscopic Fingerprints for DNA and RNA Detection. *Science*, 297(5586), 1536 LP-1540. Retrieved from <http://science.sciencemag.org/content/297/5586/1536.abstract>
- Chen, X., Zhu, H., Zhao, J., Zheng, Z., & Gao, X. (2008). Visible-Light-Driven Oxidation of Organic Contaminants in Air with Gold Nanoparticle Catalysts on Oxide Supports. *Angewandte Chemie International Edition*, 47(29), 5353–5356. <https://doi.org/10.1002/anie.200800602>
- Cheng, J. Y., Mayes, A. M., & Ross, C. A. (2004). Nanostructure engineering by

- templated self-assembly of block copolymers. *Nature Materials*, 3(11), 823–828. <https://doi.org/10.1038/nmat1211>
- Dew, S. K., & Stepanova, M. (2012). Directions in Nanofabrication. In *Nanofabrication* (pp. 3–8). Vienna: Springer Vienna. [https://doi.org/10.1007/978-3-7091-0424-8\\_1](https://doi.org/10.1007/978-3-7091-0424-8_1)
- Dey, S., & Zhao, J. (2016). Plasmonic Effect on Exciton and Multiexciton Emission of Single Quantum Dots. *The Journal of Physical Chemistry Letters*, 7(15), 2921–2929. <https://doi.org/10.1021/acs.jpcllett.6b01164>
- Dieringer, J. A., McFarland, A. D., Shah, N. C., Stuart, D. A., Whitney, A. V, Yonzon, C. R., ... Van Duyne, R. P. (2006). Surface enhanced Raman spectroscopy: new materials, concepts, characterization tools, and applications. *Faraday Discussions*, 132, 9–26. Retrieved from <http://www.ncbi.nlm.nih.gov/pubmed/16833104>
- Doktycz, S. J., & Suslick, K. S. (1990). Interparticle collisions driven by ultrasound. *Science (New York, N.Y.)*, 247(4946), 1067–1069. <https://doi.org/10.1126/science.2309118>
- Farjami, E., Clima, L., Gothelf, K. V., & Ferapontova, E. E. (2010). DNA interactions with a Methylene Blue redox indicator depend on the DNA length and are sequence specific. *The Analyst*, 135(6), 1443. <https://doi.org/10.1039/c0an00049c>
- Giljohann, D. A., Seferos, D. S., Daniel, W. L., Massich, M. D., Patel, P. C., & Mirkin, C. A. (2010). Gold Nanoparticles for Biology and Medicine. *Angewandte Chemie International Edition*, 49(19), 3280–3294. <https://doi.org/10.1002/anie.200904359>
- Haynes, C. L., McFarland, A. D., & Duyne, R. P. Van. (2005). Surface-Enhanced Raman Spectroscopy. *Analytical Chemistry*, 77(17), 338 A-346 A. <https://doi.org/10.1021/ac053456d>
- Homola, J., Yee, S. S., & Gauglitz, G. (1999). Surface plasmon resonance sensors: review. *Sensors and Actuators B: Chemical*, 54(1–2), 3–15. [https://doi.org/10.1016/S0925-4005\(98\)00321-9](https://doi.org/10.1016/S0925-4005(98)00321-9)
- Jalili, N., & Laxminarayana, K. (2004). A review of atomic force microscopy imaging systems: application to molecular metrology and biological sciences. *Mechatronics*, 14(8), 907–945. <https://doi.org/10.1016/J.MECHATRONICS.2004.04.005>
- Kelly, P. ., & Arnell, R. . (2000). Magnetron sputtering: a review of recent developments and applications. *Vacuum*, 56(3), 159–172. [https://doi.org/10.1016/S0042-207X\(99\)00189-X](https://doi.org/10.1016/S0042-207X(99)00189-X)
- Kim, S. M., Lee, S. W., Moon, S. Y., & Park, J. Y. (2016a). The effect of hot electrons and surface plasmons on heterogeneous catalysis. *Journal of Physics: Condensed Matter*, 28(25), 254002. <https://doi.org/10.1088/0953-8984/28/25/254002>

- Kim, S. M., Lee, S. W., Moon, S. Y., & Park, J. Y. (2016b). The effect of hot electrons and surface plasmons on heterogeneous catalysis. *Journal of Physics: Condensed Matter*, 28(25), 254002. <https://doi.org/10.1088/0953-8984/28/25/254002>
- Knight, D. S., & White, W. B. (1989). Characterization of diamond films by Raman spectroscopy. *Journal of Materials Research*, 4(02), 385–393. <https://doi.org/10.1557/JMR.1989.0385>
- Kulkarni, A. P., Noone, K. M., Munechika, K., Guyer, S. R., & Ginger, D. S. (2010). Plasmon-Enhanced Charge Carrier Generation in Organic Photovoltaic Films Using Silver Nanoprisms. *Nano Letters*, 10(4), 1501–1505. <https://doi.org/10.1021/nl100615e>
- Lal, S., Grady, N. K., Kundu, J., Levin, C. S., Lassiter, J. B., & Halas, N. J. (2008). Tailoring plasmonic substrates for surface enhanced spectroscopies. *Chemical Society Reviews*, 37(5), 898. <https://doi.org/10.1039/b705969h>
- Li, T., Wu, X., Tao, G., Yin, H., Zhang, J., Liu, F., & Li, N. (2018). A simple and non-amplification platform for femtomolar DNA and microRNA detection by combining automatic gold nanoparticle enumeration with target-induced strand-displacement. *Biosensors and Bioelectronics*, 105, 137–142. <https://doi.org/10.1016/j.bios.2018.01.034>
- Liu, D., Yang, D., Gao, Y., Ma, J., Long, R., Wang, C., & Xiong, Y. (2016). Flexible Near-Infrared Photovoltaic Devices Based on Plasmonic Hot-Electron Injection into Silicon Nanowire Arrays. *Angewandte Chemie*, 128(14), 4653–4657. <https://doi.org/10.1002/ange.201600279>
- Liu, H., Zhang, L., Lang, X., Yamaguchi, Y., Iwasaki, H., Inouye, Y., ... Chen, M. (2011). Single molecule detection from a large-scale SERS-active Au<sub>79</sub>Ag<sub>21</sub> substrate. *Scientific Reports*, 1(1), 112. <https://doi.org/10.1038/srep00112>
- Meyer, E. (1992). Atomic force microscopy. *Progress in Surface Science*, 41(1), 3–49. [https://doi.org/10.1016/0079-6816\(92\)90009-7](https://doi.org/10.1016/0079-6816(92)90009-7)
- Mirkin, C. A., Letsinger, R. L., Mucic, R. C., & Storhoff, J. J. (1996). A DNA-based method for rationally assembling nanoparticles into macroscopic materials. *Nature*, 382(6592), 607–609. <https://doi.org/10.1038/382607a0>
- Mohammad, M. A., Muhammad, M., Dew, S. K., & Stepanova, M. (2012). Fundamentals of Electron Beam Exposure and Development. In *Nanofabrication* (pp. 11–41). Vienna: Springer Vienna. [https://doi.org/10.1007/978-3-7091-0424-8\\_2](https://doi.org/10.1007/978-3-7091-0424-8_2)
- Naldoni, A., Riboni, F., Guler, U., Boltasseva, A., Shalaev, V. M., & Kildishev, A. V. (2016). Solar-Powered Plasmon-Enhanced Heterogeneous Catalysis. *Nanophotonics*, 5(1), 112–133. <https://doi.org/10.1515/nanoph-2016-0018>

- Nicolai, S. H. A., & Rubim, J. C. (2003). Surface-Enhanced Resonance Raman (SERR) Spectra of Methylene Blue Adsorbed on a Silver Electrode. *Langmuir*, *19*(10), 4291–4294. <https://doi.org/10.1021/la034076v>
- Oakley, L. H., Dinehart, S. A., Svoboda, S. A., & Wustholz, K. L. (2011). Identification of Organic Materials in Historic Oil Paintings Using Correlated Extractionless Surface-Enhanced Raman Scattering and Fluorescence Microscopy. *Analytical Chemistry*, *83*(11), 3986–3989. <https://doi.org/10.1021/ac200698q>
- Papadopoulou, E., Gale, N., Thompson, J. F., Fleming, T. A., Brown, T., & Bartlett, P. N. (2016). Specifically horizontally tethered DNA probes on Au surfaces allow labelled and label-free DNA detection using SERS and electrochemically driven melting. *Chemical Science*, *7*(1), 386–393. <https://doi.org/10.1039/C5SC03185K>
- Paxton, W. F., Kleinman, S. L., Basuray, A. N., Stoddart, J. F., & Van Duyne, R. P. (2011). Surface-Enhanced Raman Spectroelectrochemistry of TTF-Modified Self-Assembled Monolayers. *The Journal of Physical Chemistry Letters*, *2*(10), 1145–1149. <https://doi.org/10.1021/jz200523q>
- Pensa, E., Cortés, E., Corthey, G., Carro, P., Vericat, C., Fonticelli, M. H., ... Salvarezza, R. C. (2012). The Chemistry of the Sulfur–Gold Interface: In Search of a Unified Model. *Accounts of Chemical Research*, *45*(8), 1183–1192. <https://doi.org/10.1021/ar200260p>
- Persson, B. N. J., & Ryberg, R. (1981). Vibrational interaction between molecules adsorbed on a metal surface: The dipole-dipole interaction. *Physical Review B*, *24*(12), 6954–6970. <https://doi.org/10.1103/PhysRevB.24.6954>
- Peters, R. F., Gutierrez-Rivera, L., Dew, S. K., & Stepanova, M. (2015). Surface Enhanced Raman Spectroscopy Detection of Biomolecules Using EBL Fabricated Nanostructured Substrates. *Journal of Visualized Experiments*, (97), e52712–e52712. <https://doi.org/10.3791/52712>
- Raman, C. V., & Krishnan, K. S. (1928). A New Type of Secondary Radiation. *Nature*, *121*(3048), 501–502. <https://doi.org/10.1038/121501c0>
- Ravindran, A., Chandran, P., & Khan, S. S. (2013). Biofunctionalized silver nanoparticles: Advances and prospects. *Colloids and Surfaces B: Biointerfaces*, *105*, 342–352. <https://doi.org/10.1016/j.colsurfb.2012.07.036>
- Roh, J. Y., Matecki, M. K., Svoboda, S. A., & Wustholz, K. L. (2016). Identifying Pigment Mixtures in Art Using SERS: A Treatment Flowchart Approach. *Analytical Chemistry*, *88*(4), 2028–2032. <https://doi.org/10.1021/acs.analchem.6b00044>
- Sharma, B., Frontiera, R. R., Henry, A.-I., Ringe, E., & Van Duyne, R. P. (2012). SERS: Materials, applications, and the future. *Materials Today*, *15*(1–2), 16–25.

[https://doi.org/10.1016/S1369-7021\(12\)70017-2](https://doi.org/10.1016/S1369-7021(12)70017-2)

- Sylvia, J. M., Janni, J. A., Klein, J. D., & Spencer, K. M. (2000). Surface-Enhanced Raman Detection of 2,4-Dinitrotoluene Impurity Vapor as a Marker To Locate Landmines. *Analytical Chemistry*, 72(23), 5834–5840.  
<https://doi.org/10.1021/ac0006573>
- Thornton, J. A. (1978). Magnetron sputtering: basic physics and application to cylindrical magnetrons. *Journal of Vacuum Science and Technology*, 15(2), 171–177.  
<https://doi.org/10.1116/1.569448>
- Vardevanyan, P. O., Antonyan, A. P., Parsadanyan, M. A., Shahinyan, M. A., & Hambarzumyan, L. A. (2013). Mechanisms for Binding between Methylene Blue and DNA. *Journal of Applied Spectroscopy*, 80(4), 595–599.  
<https://doi.org/10.1007/s10812-013-9811-7>
- Weitz, D. A., Garoff, S., Gersten, J. I., & Nitzan, A. (1983). The enhancement of Raman scattering, resonance Raman scattering, and fluorescence from molecules adsorbed on a rough silver surface. *The Journal of Chemical Physics*, 78(9), 5324–5338.  
<https://doi.org/10.1063/1.445486>
- Wu, K., Chen, J., McBride, J. R., & Lian, T. (2015). Efficient hot-electron transfer by a plasmon-induced interfacial charge-transfer transition. *Science*, 349(6248), 632–635.  
<https://doi.org/10.1126/science.aac5443>
- Xiao, G.-N., & Man, S.-Q. (2007). Surface-enhanced Raman scattering of methylene blue adsorbed on cap-shaped silver nanoparticles. *Chemical Physics Letters*, 447(4–6), 305–309. <https://doi.org/10.1016/J.CPLETT.2007.09.045>
- Xie, W., & Schlücker, S. (2014). Rationally designed multifunctional plasmonic nanostructures for surface-enhanced Raman spectroscopy: a review. *Reports on Progress in Physics*, 77(11), 116502. <https://doi.org/10.1088/0034-4885/77/11/116502>
- Yagi, N., Satonaka, K., Horio, M., Shimogaki, H., Tokuda, Y., & Maeda, S. (1996). The Role of DNase and EDTA on DNA Degradation in Formaldehyde Fixed Tissues. *Biotechnic & Histochemistry*, 71(3), 123–129.  
<https://doi.org/10.3109/10520299609117148>
- Ye, W., Long, R., Huang, H., & Xiong, Y. (2017). Plasmonic nanostructures in solar energy conversion. *Journal of Materials Chemistry C*, 5(5), 1008–1021.  
<https://doi.org/10.1039/C6TC04847A>
- Zeng, Z., Liu, Y., & Wei, J. (2016). Recent advances in surface-enhanced Raman spectroscopy (SERS): Finite-difference time-domain (FDTD) method for SERS and sensing applications. *TrAC Trends in Analytical Chemistry*, 75, 162–173.

<https://doi.org/10.1016/J.TRAC.2015.06.009>